Electronic Supplementary Material (ESI) for Journal of Materials Chemistry A.
This journal is © The Royal Society of Chemistry 2021

Electronic Supplementary material for

Accurately Metal-Modulated Bimetallic Metal-Organic Frameworks as an Advanced Trifunctional Electrocatalyst

Xin Chen,[1] Bing Shao,[1] Meng-Juan Tang,[1] Xing-Lu He,[1] Fu-Jie Yang,[3] Ze-Ping Guo,[4] Zhong Zhang,[1] Chun-Ting He,*[2] Fu-Ping Huang,*[1] Jin Huang*[1]

[1]*School of Chemistry and Pharmacy, Guangxi Normal University, Guilin 541004, P. R. China*

[2]*Key Laboratory of Functional Small Organic Molecule, Ministry of Education, College of Chemistry and Chemical Engineering, Jiangxi Normal University, Nanchang 330022, China*

[3]*College Chemistry and Chemical Engineering, Zhongkai University of Agriculture and Engineering, Guangzhou 510275, P. R. China*

[4]*School of Physical Science and Technology, Guangxi Normal University, Guilin 541004, P. R. China*

*E-mail: hct@jxnu.edu.cn, huangfp2010@163.com, huangjin@mailbox.gxnu.edu.cn

(a)

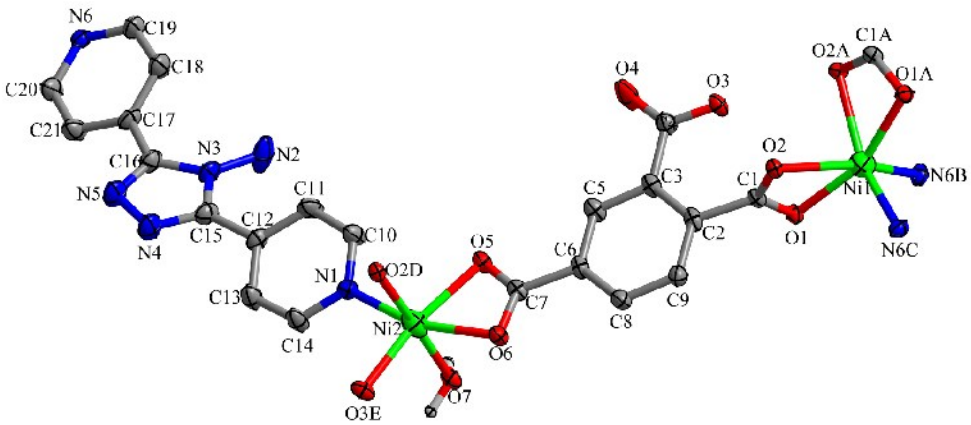

(b)

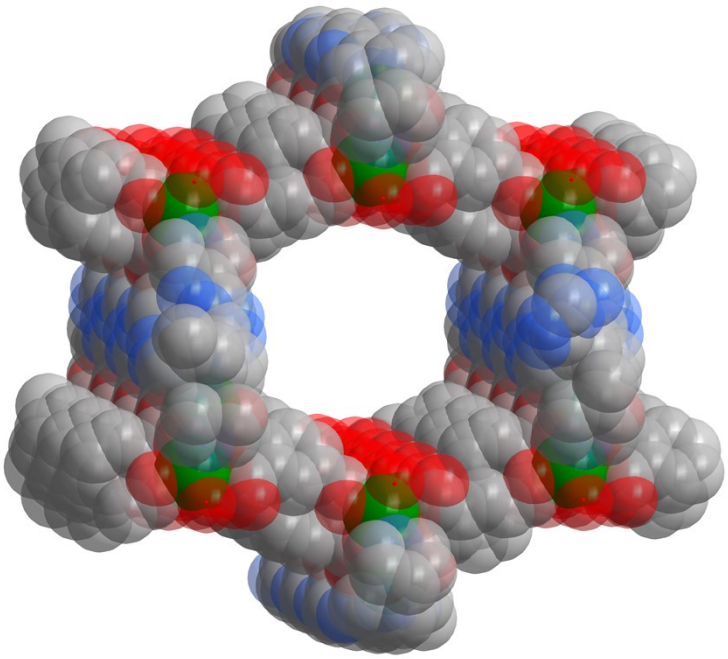

Figure S1. (a) The asymmetric unit of **Ni_3-MOF** (Symmetry codes: A = -x+1, y, -z-1/2; B = -x-1/2, y-1/2, -z-1/2; C = x+3/2, y-1/2, z; D = -x+1/2, -y+1/2, -z; E = x-1/2, -y+1/2, z+1/2, hydrogen atoms and guest molecule are omitted for clarity). (b) Three-dimensional structure of **Ni_3-MOF**.

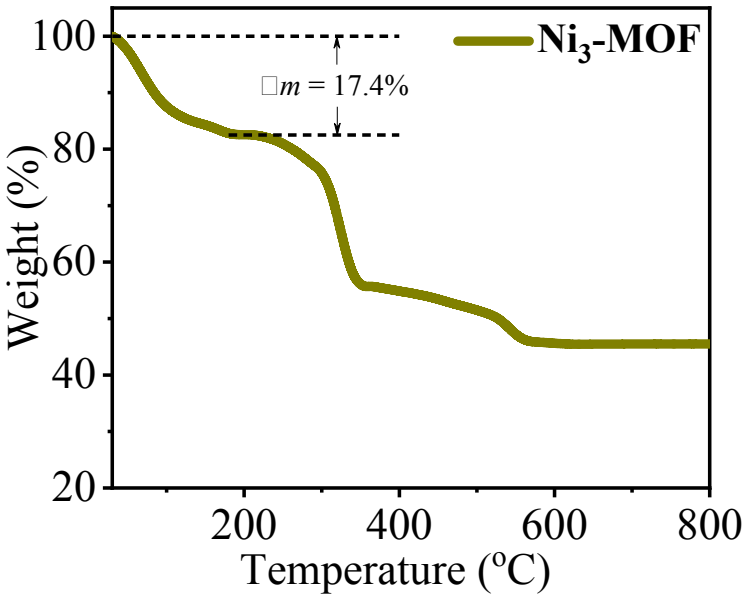

Figure S2. Thermogravimetry curve of **Ni_3-MOF** measured at N_2 atmosphere.

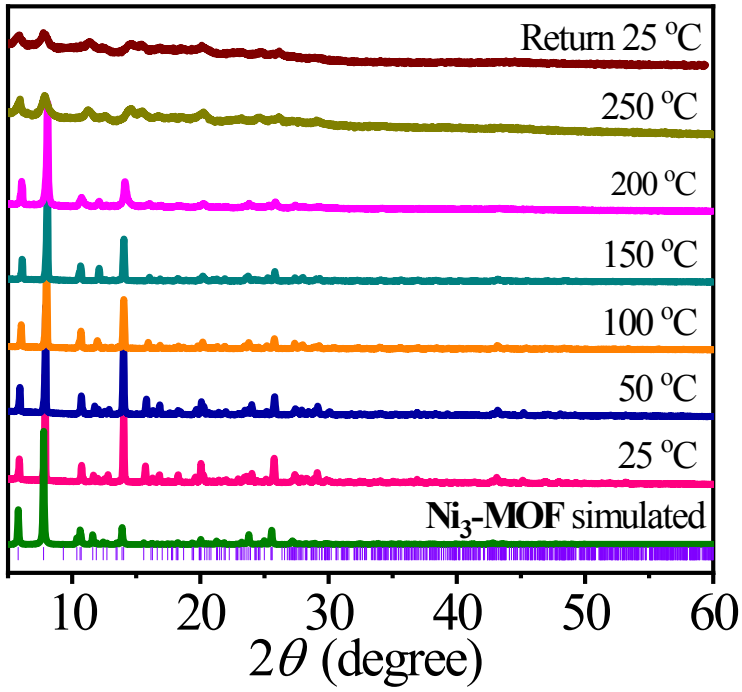

Figure S3. In-situ warm-keeping PXRD patterns of **Ni_3-MOF** under N_2 atmosphere.

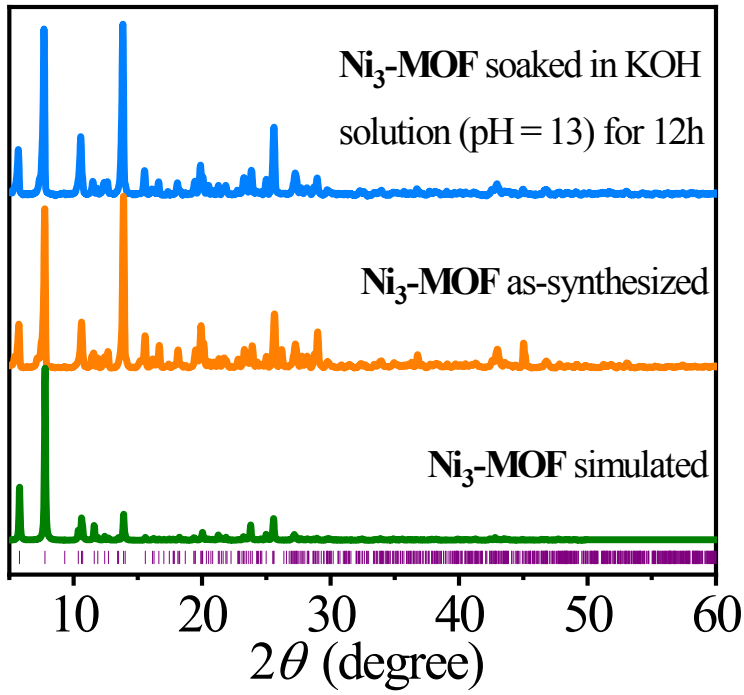

Figure S4. PXRD patterns of **Ni_3-MOF** in 0.1 M KOH solution (pH = 13).

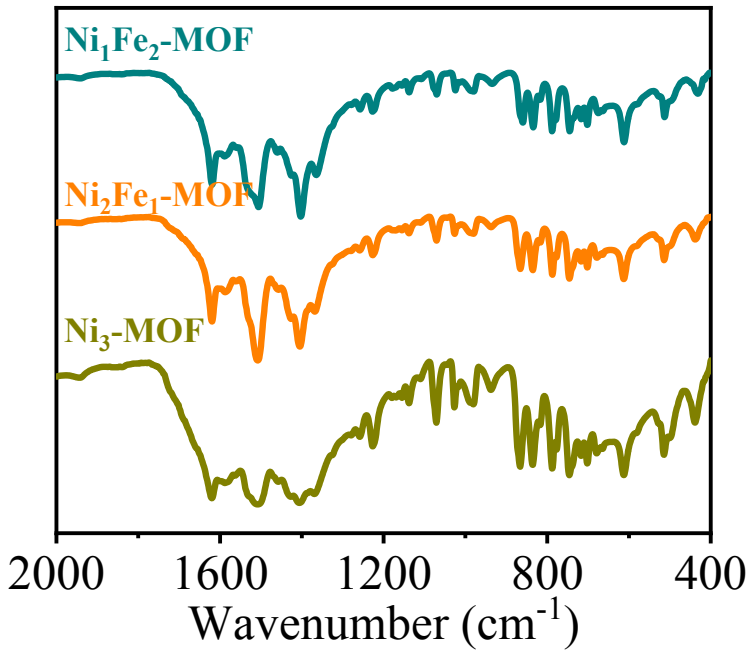

Figure S5. Infrared spectra of **Ni_3-MOF**, **Ni_2Fe_1-MOF** and **Ni_1Fe_2-MOF**.

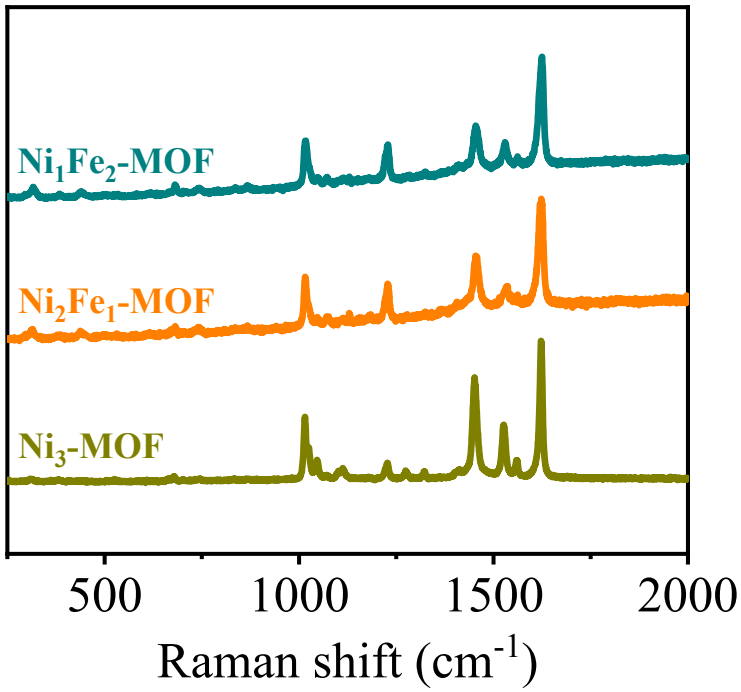

Figure S6. Raman spectra of **Ni_3-MOF**, **Ni_2Fe_1-MOF** and **Ni_1Fe_2-MOF**.

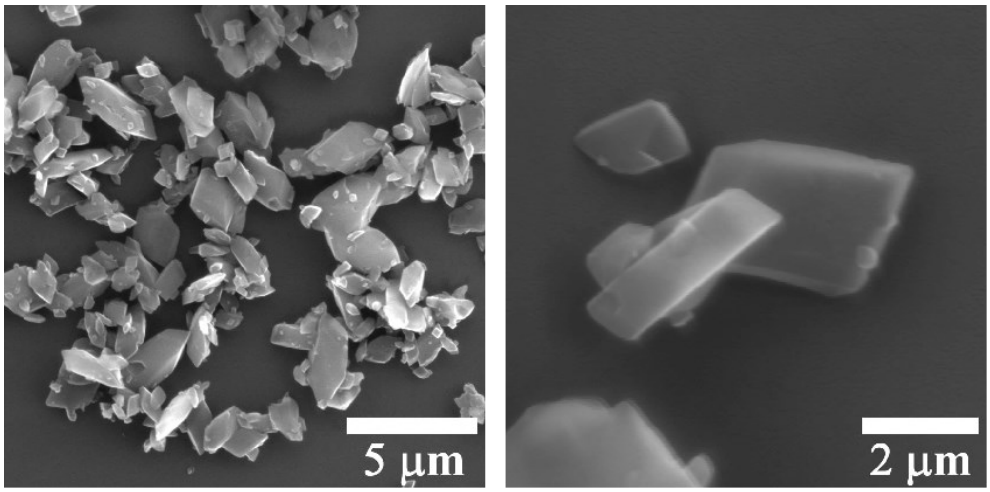

Figure S7. SEM images of **Ni_3-MOF**.

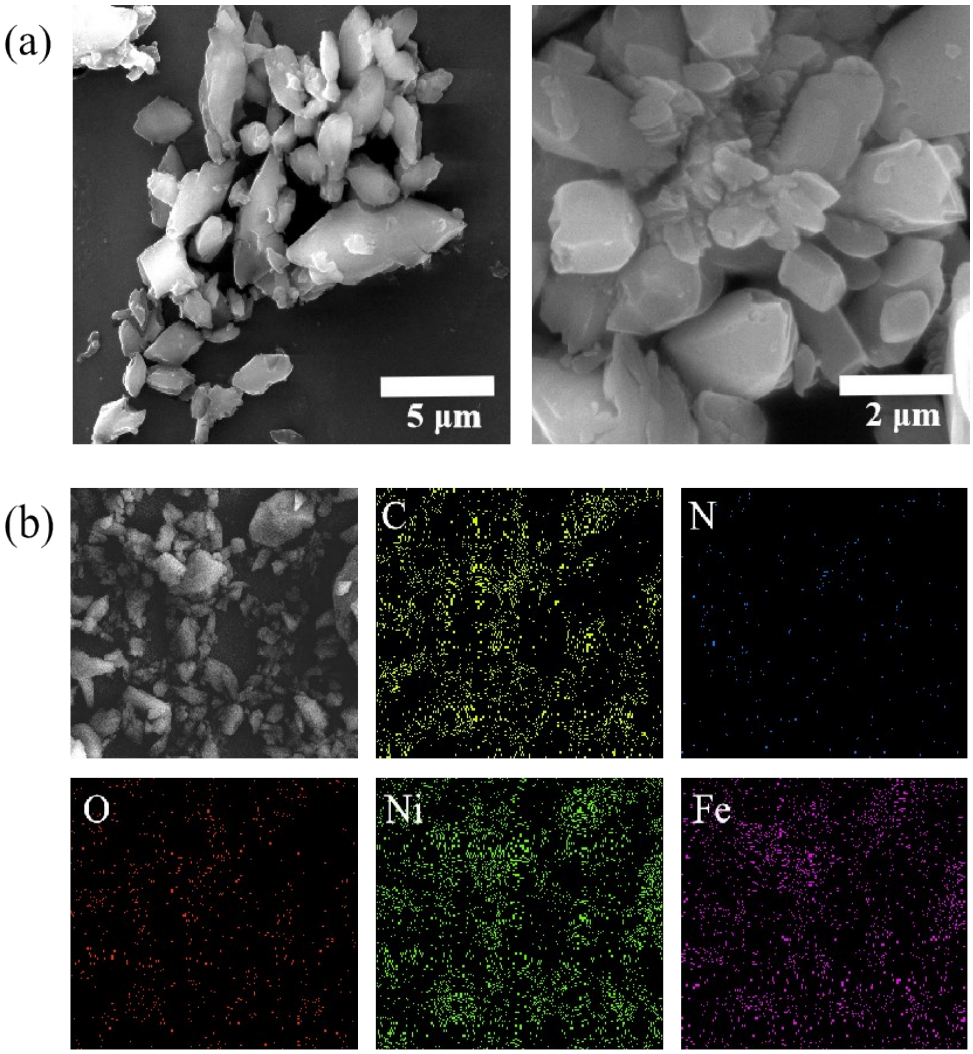

Figure S8. (a) SEM images of **Ni_2Fe_1-MOF**. (b) SEM-EDS mapping images of **Ni_2Fe_1-MOF**.

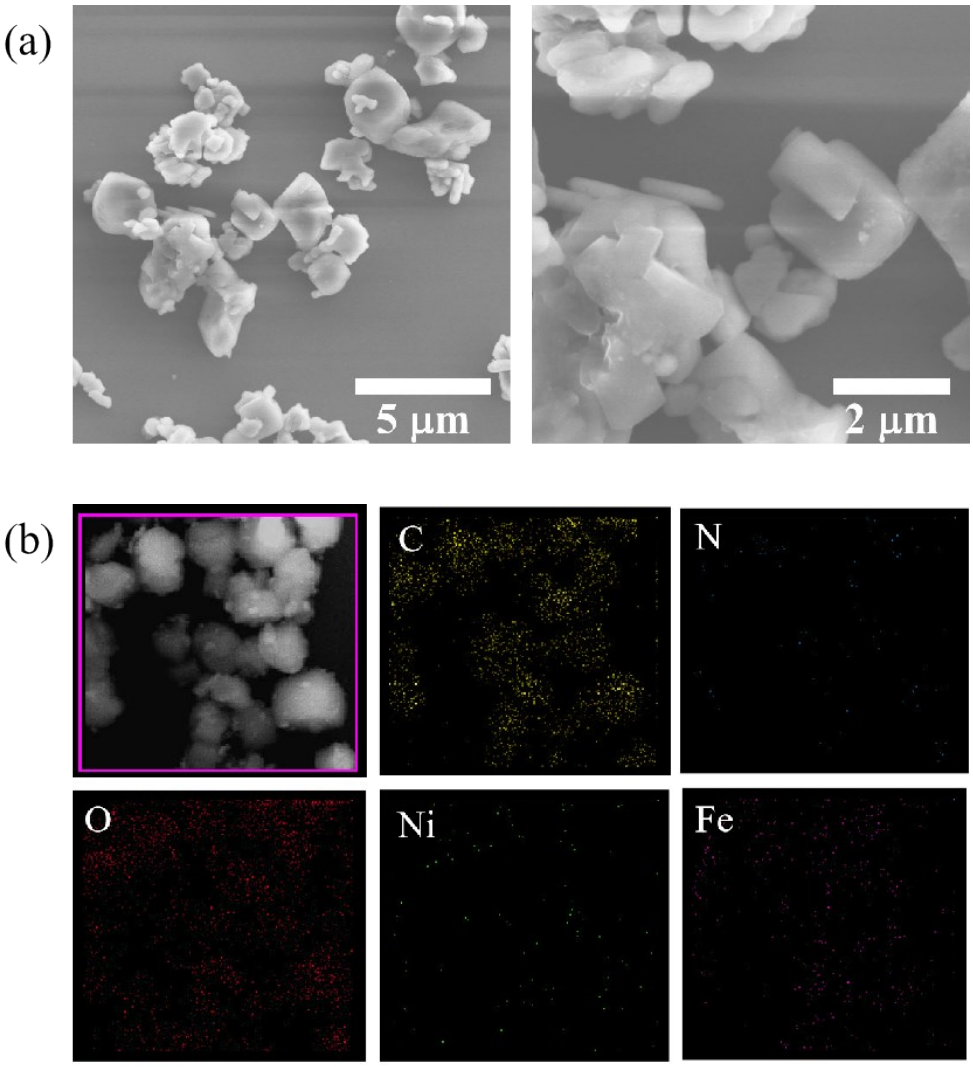

Figure S9. (a) SEM images of **Ni_1Fe_2-MOF**. (b) SEM-EDS mapping images of **Ni_1Fe_2-MOF**.

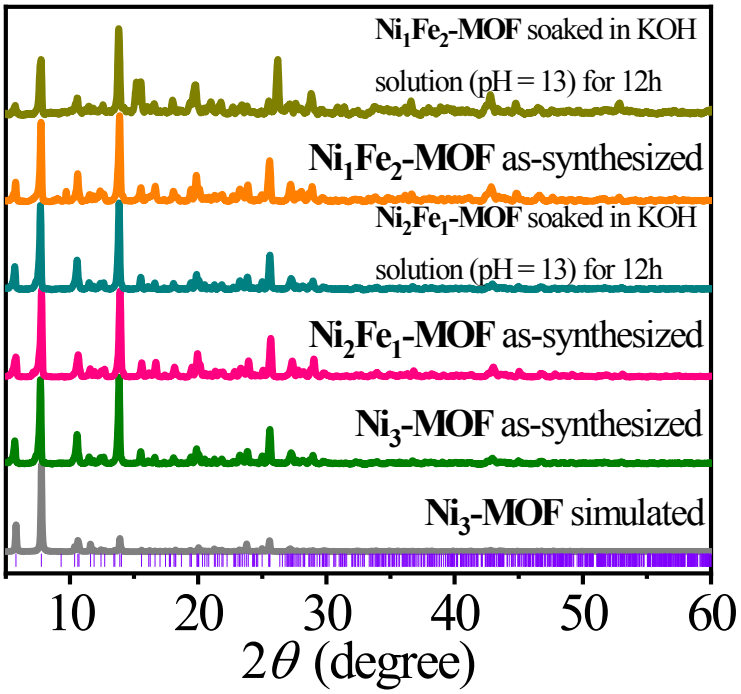

Figure S10. PXRD patterns of $\mathbf{Ni_{3(1-x)}Fe_{3x}}$**-MOF** in 0.1 M KOH solution (pH = 13).

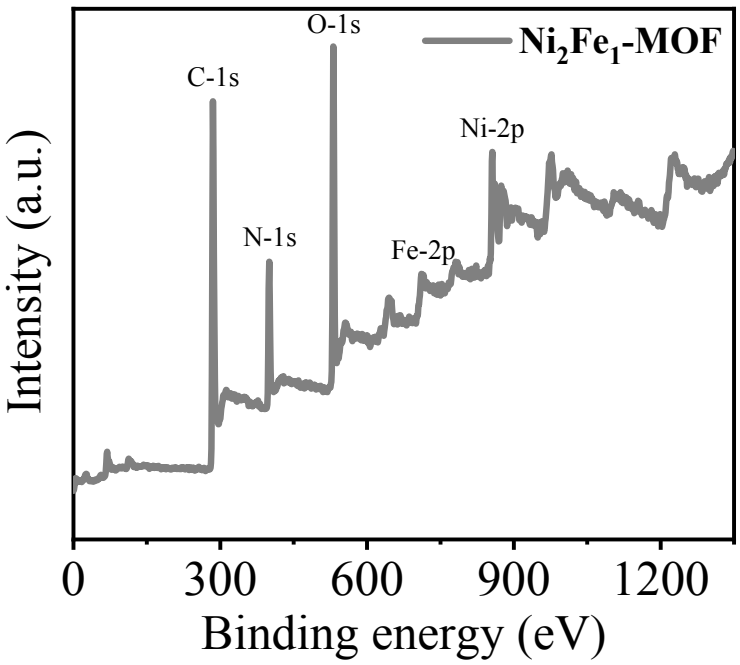

Figure S11. XPS summary spectra of $\mathbf{Ni_2Fe_1}$**-MOF**.

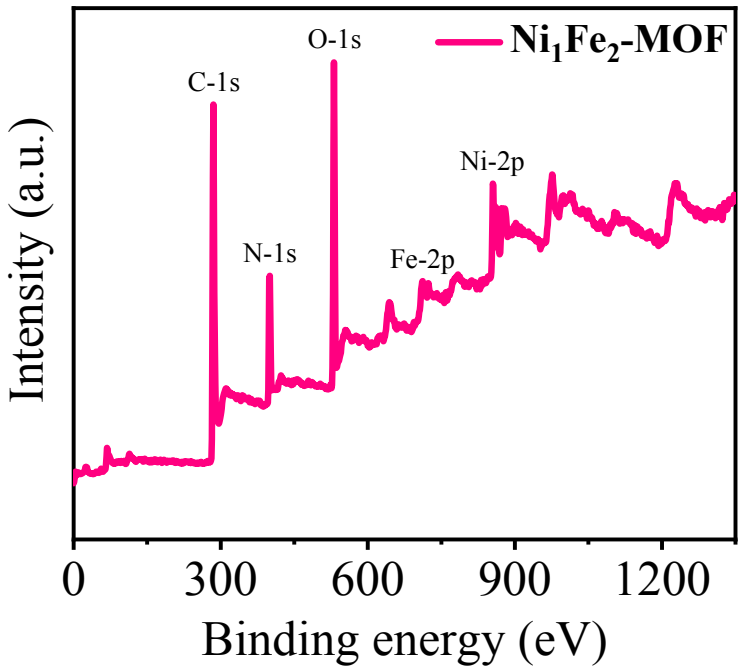

Figure S12. XPS summary spectra of **Ni_1Fe_2-MOF**.

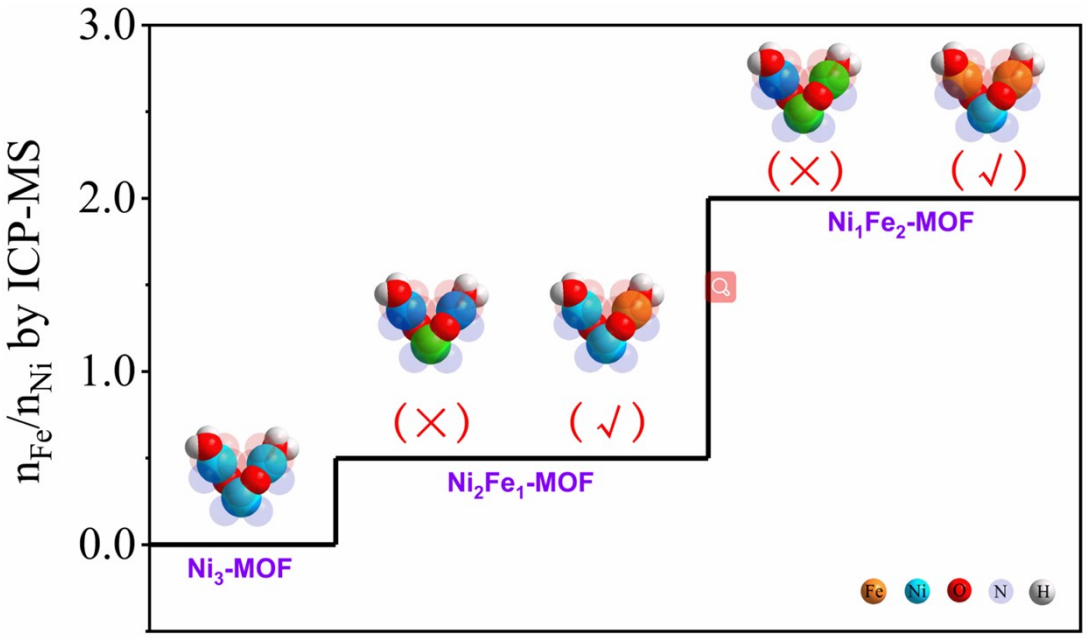

Figure S13. The diagram of V-shaped tri-nuclear cluster in **$Ni_{3(1-x)}Fe_{3x}$-MOF** (x = 0, 0.33, 0.67).

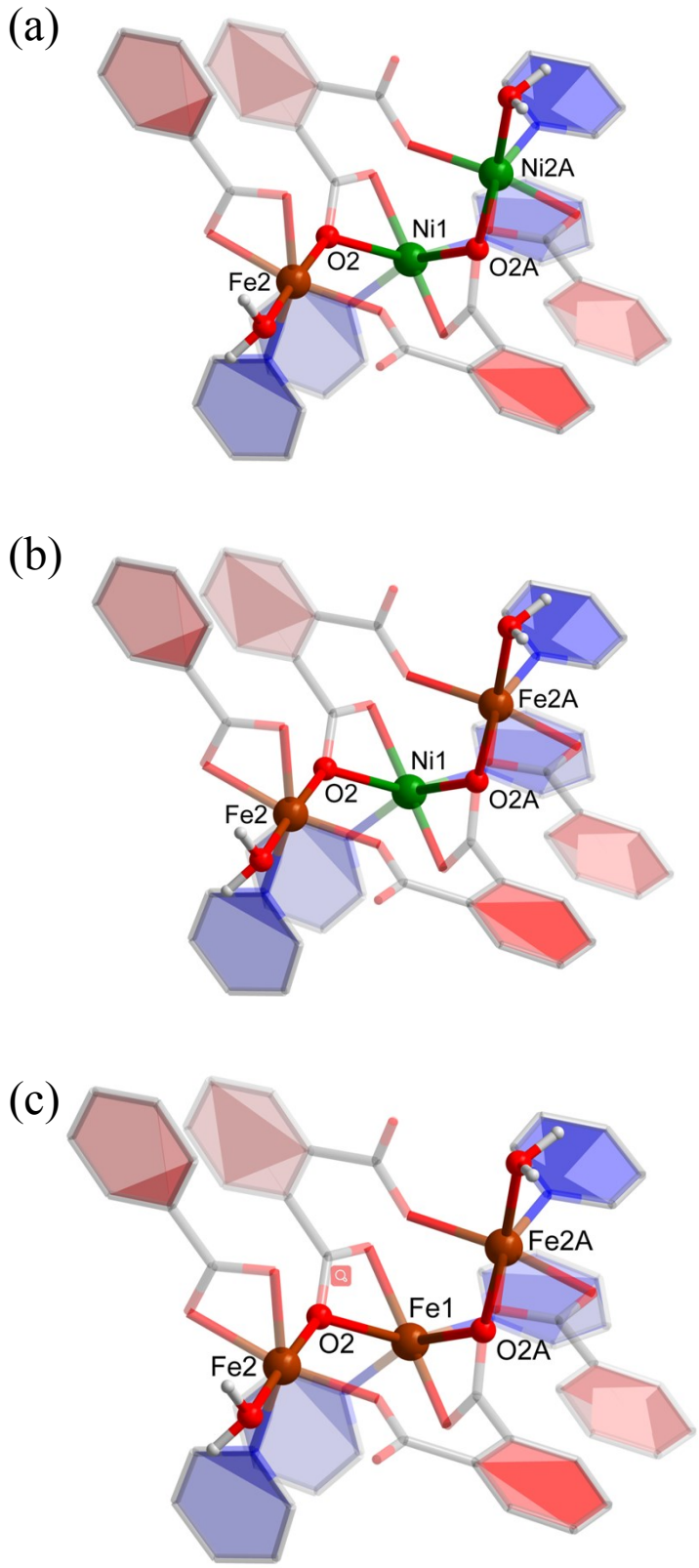

Figure S14. Coordination environment of V-shaped trinuclear clusters in the (a) **Fe_1-MOF**, (b) **Ni_1Fe_2-MOF** and (c) **$NiFe_3$-MOF**.

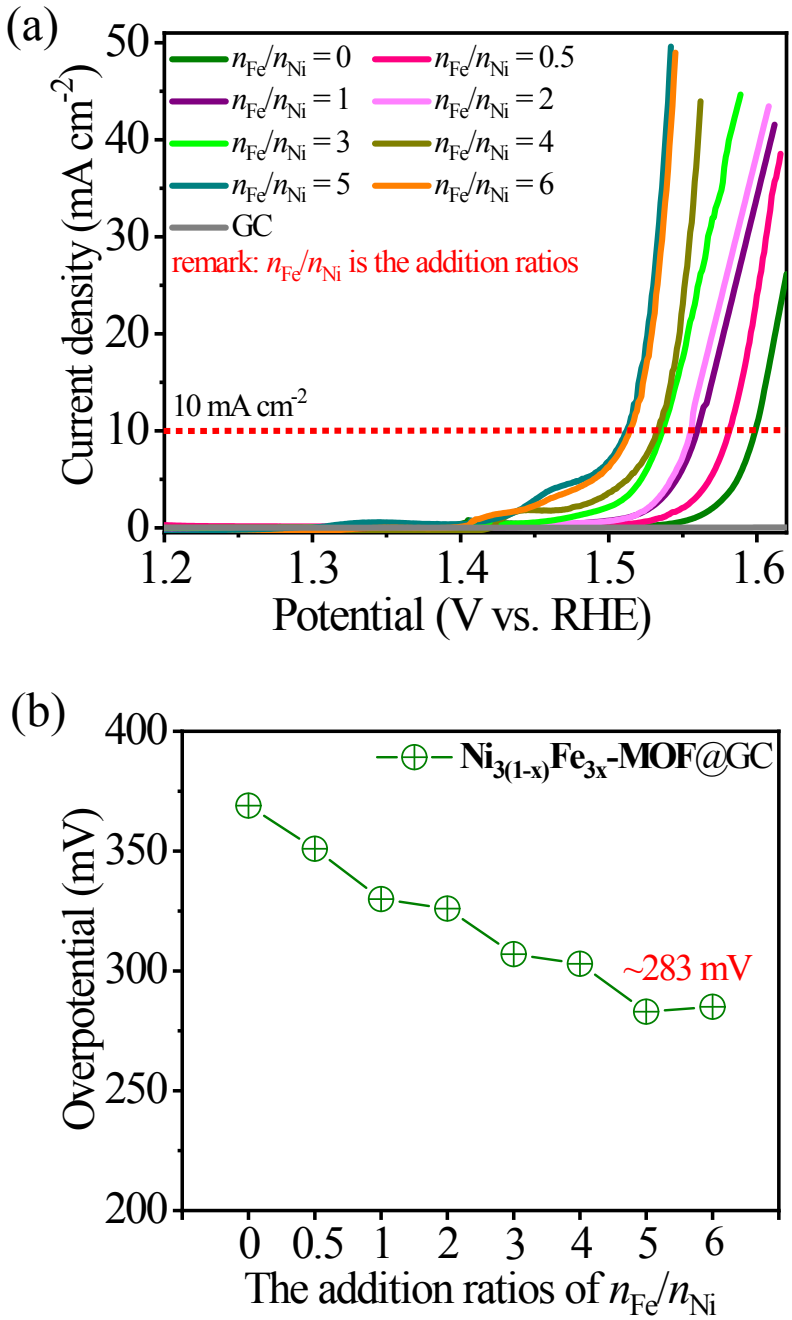

Figure S15. (a) LSV OER curves and (b) the corresponding η_{OER-10} of **$Ni_{3(1-x)}Fe_{3x}$-MOF**@GC in 0.1m KOH solution (pH 13).

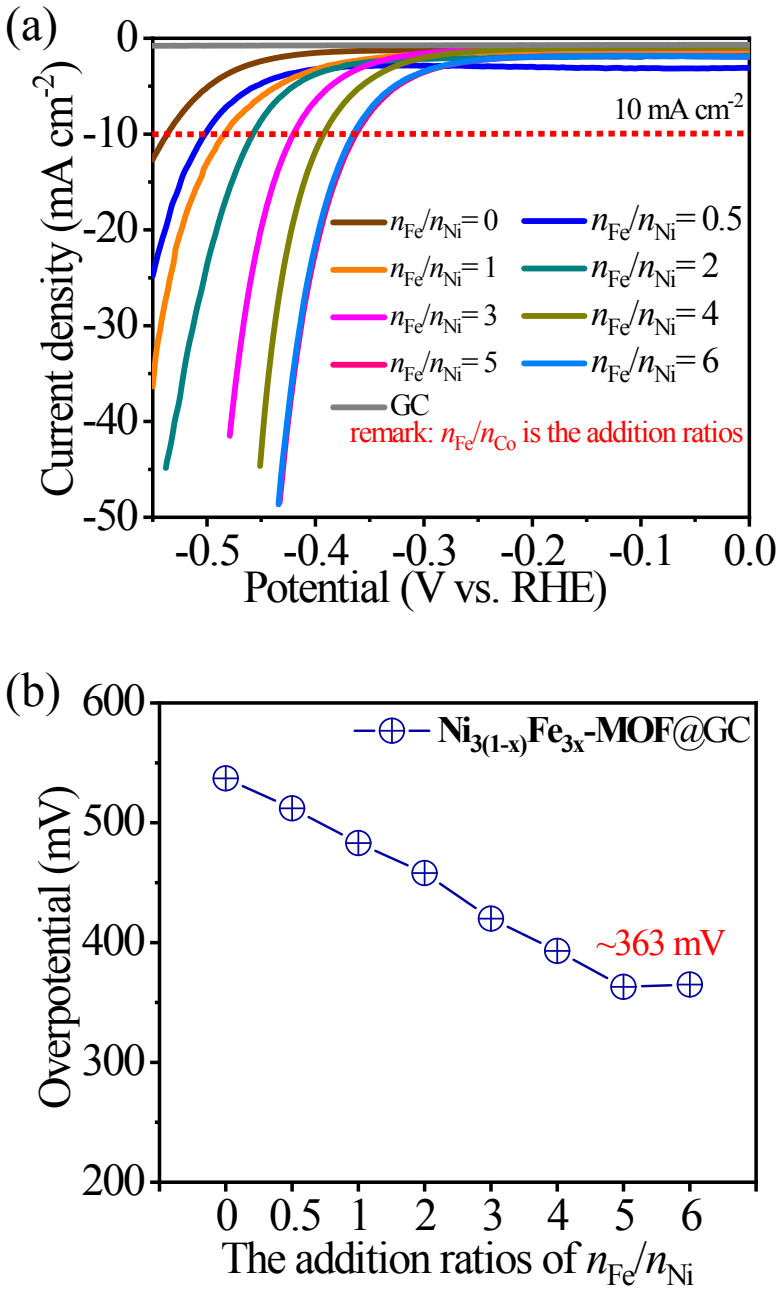

Figure S16. (a) LSV HER curves and (b) the corresponding η_{HER-10} of **$Ni_{3(1-x)}Fe_{3x}$-MOF**@GC in 0.1m KOH solution (pH 13).

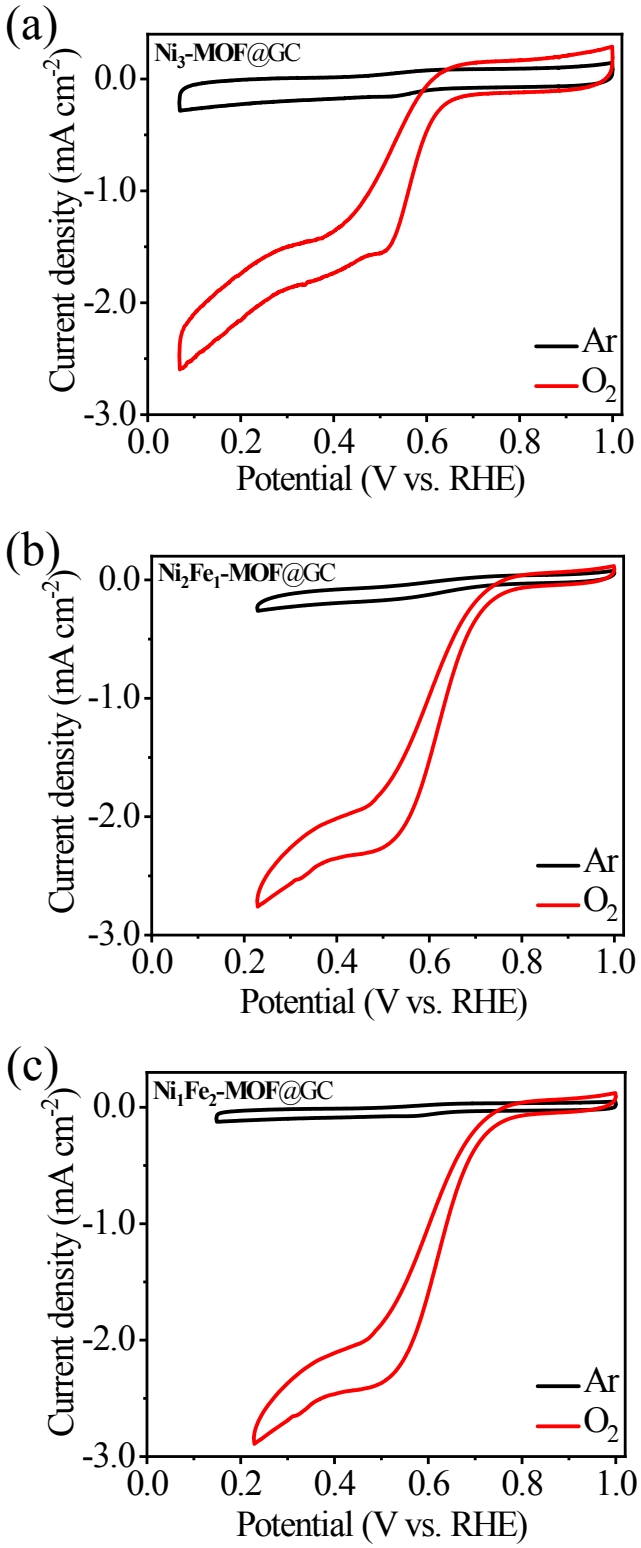

Figure S17. CV curve of (a) **Ni_3-MOF**@GC, (b) **Ni_2Fe_1-MOF**@GC, and (c) **Ni_1Fe_2-MOF**@GC in O_2-saturated/Ar-saturated 0.1 M KOH solution.

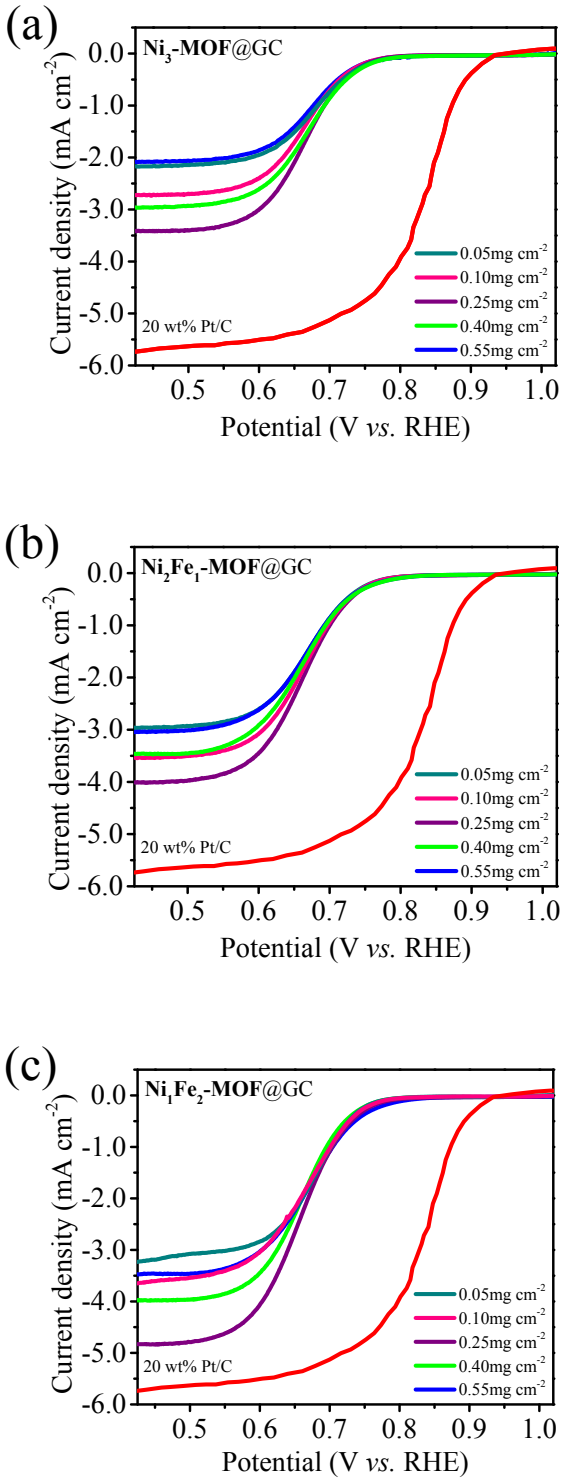

Figure S18. LSV curves at different mass loading of (a) **Ni_3-MOF**@GC, (b) **Ni_2Fe_1-MOF**@GC, and (c) **Ni_1Fe_2-MOF**@GC at 2500 r.p.m. in O_2-saturated 0.1 M. The LSV curves of 20% Pt/C refer to *Nat. Energy* **2016**, *1,* 15006.

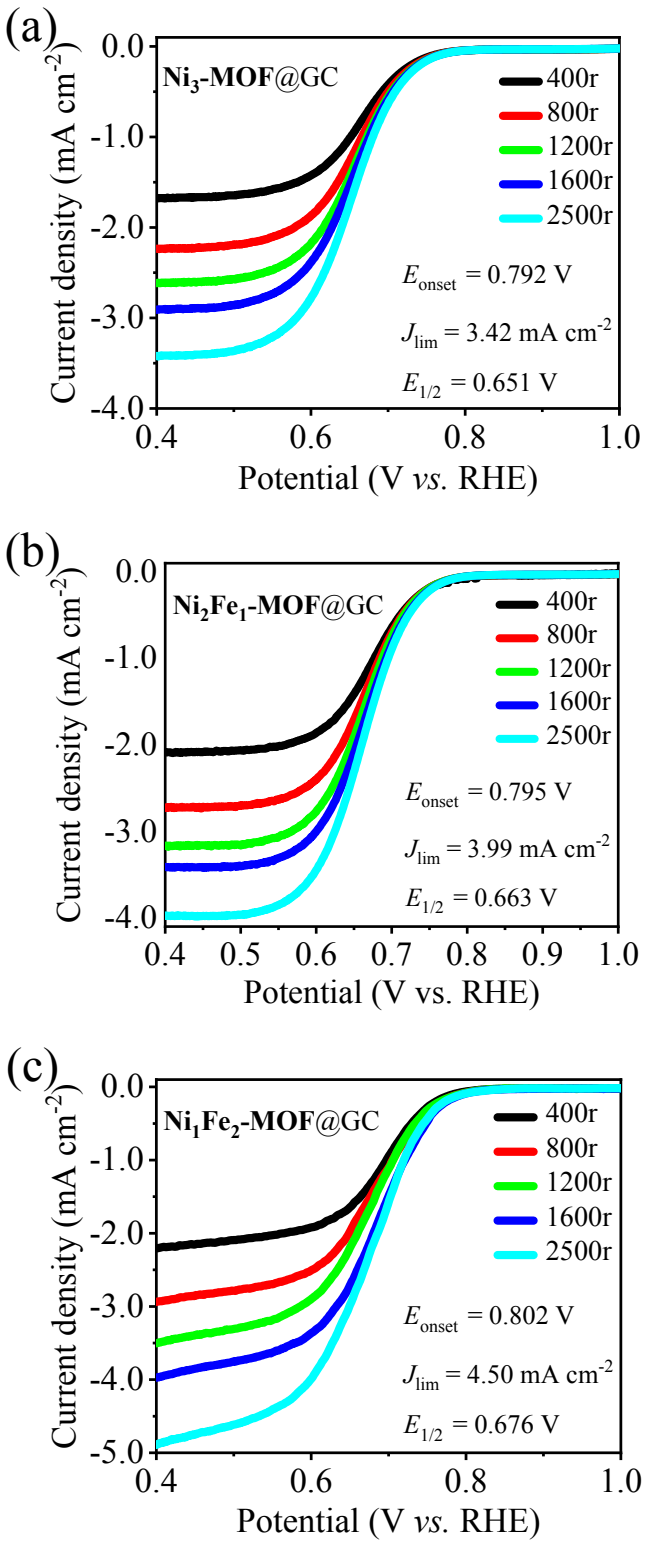

Figure S19. LSV curves at different rotation rates (r.p.m.) of (a) **Ni_3-MOF**@GC, (b) **Ni_2Fe_1-MOF**@GC, and (c) **Ni_1Fe_2-MOF**@GC in O_2-saturated 0.1 M KOH solution.

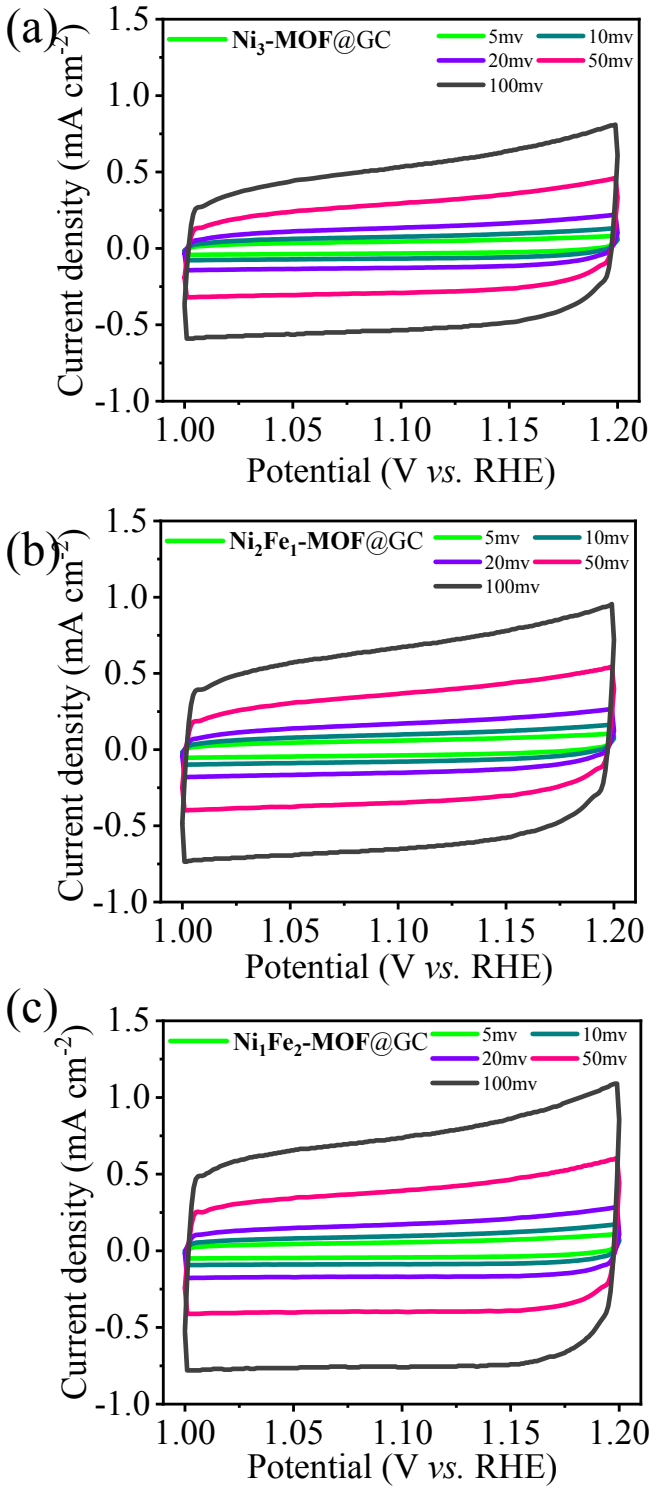

Figure S20. CV curves of in double layer region at scan rates of 5 mV s^{-1}, 10 mV s^{-1}, 20 mV s^{-1}, 50 mV s^{-1} and 100 mV s^{-1} of (a) **Ni_3-MOF**@GC, (b) **Ni_2Fe_1-MOF**@GC, and (c) **Ni_1Fe_2-MOF**@GC.

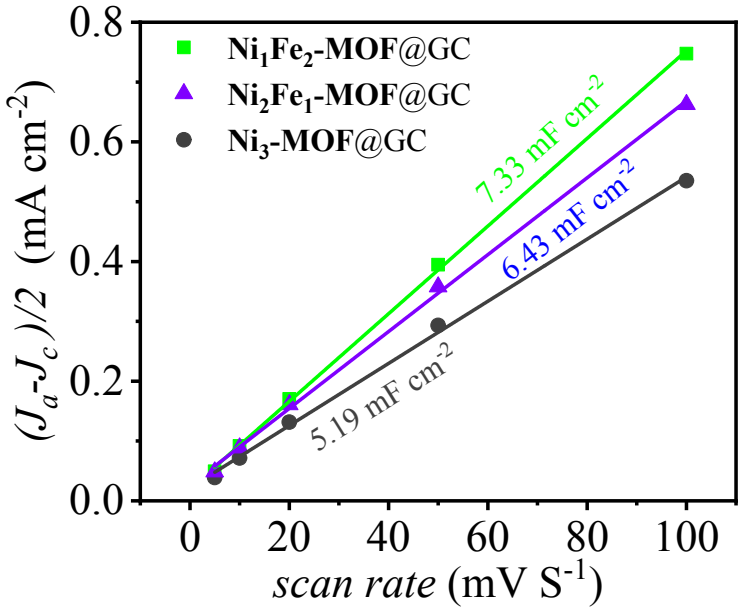

Figure S21. Current density as a function of the scan rate for **Ni_3-MOF**@GC, **Ni_2Fe_1-MOF**@GC, and **Ni_1Fe_2-MOF**@GC, used to indicate the electrochemically active surface area.

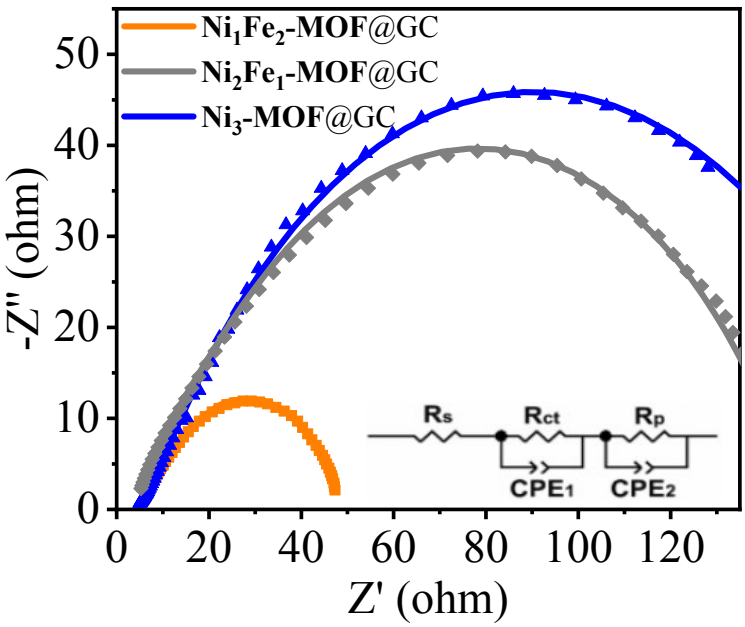

Figure S22. Nyquist plots of **Ni_3-MOF**@GC, **Ni_2Fe_1-MOF**@GC, and **Ni_1Fe_2-MOF**@GC.

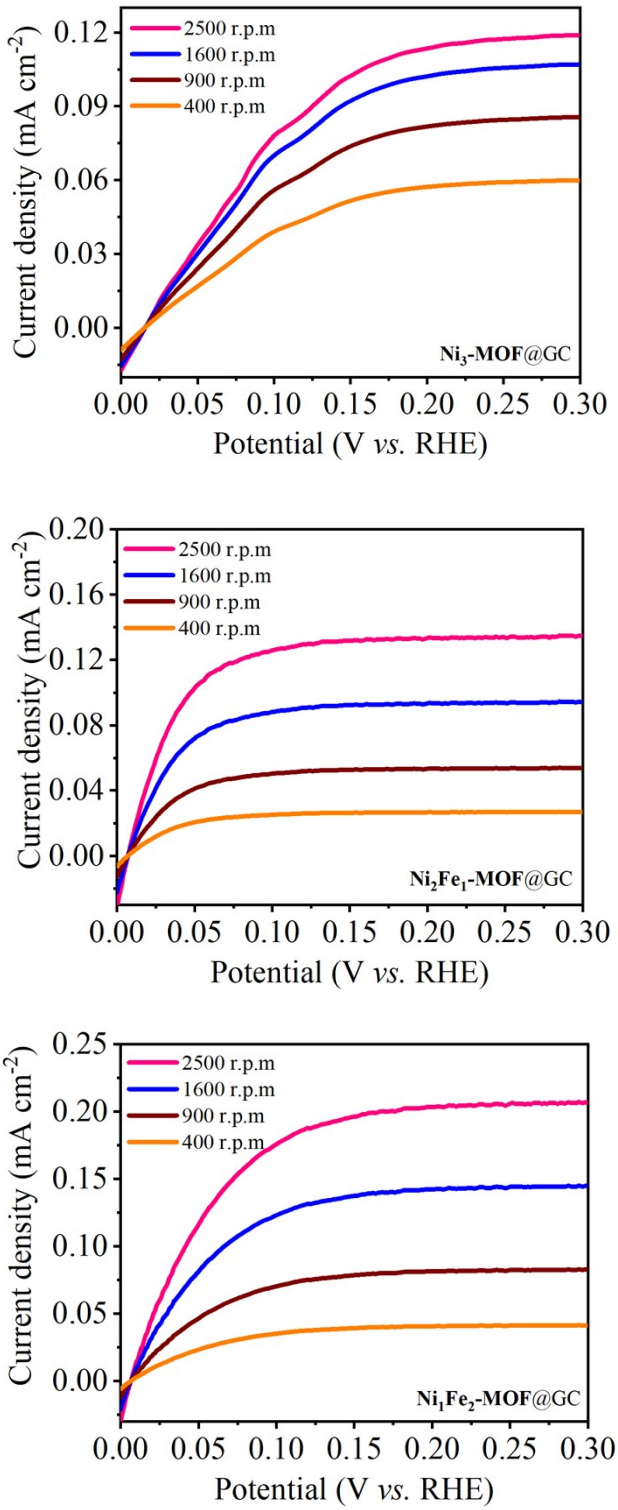

Figure S23. LSV curves at different rotation rates (r.p.m.) of (a) **Ni_3-MOF**@GC, (b) **Ni_2Fe_1-MOF**@GC, and (c) **Ni_1Fe_2-MOF**@GC in H_2-saturated 0.1 M KOH solution.

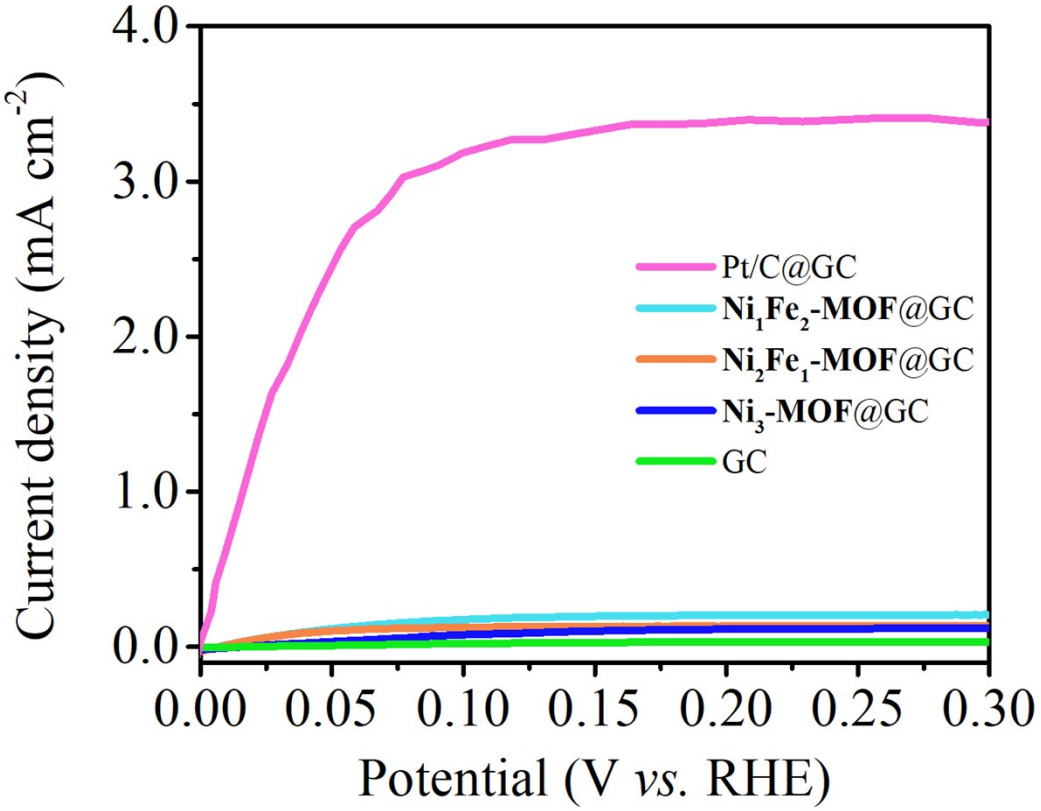

Figure S24. LSV curves at 2500 r.p.m. of **Ni_3-MOF**@GC, **Ni_2Fe_1-MOF**@GC, **Ni_1Fe_2-MOF**@GC and 20% Pt/C refer to *Angew. Chem. Int. Ed.* **2019**, *58,* 7445.

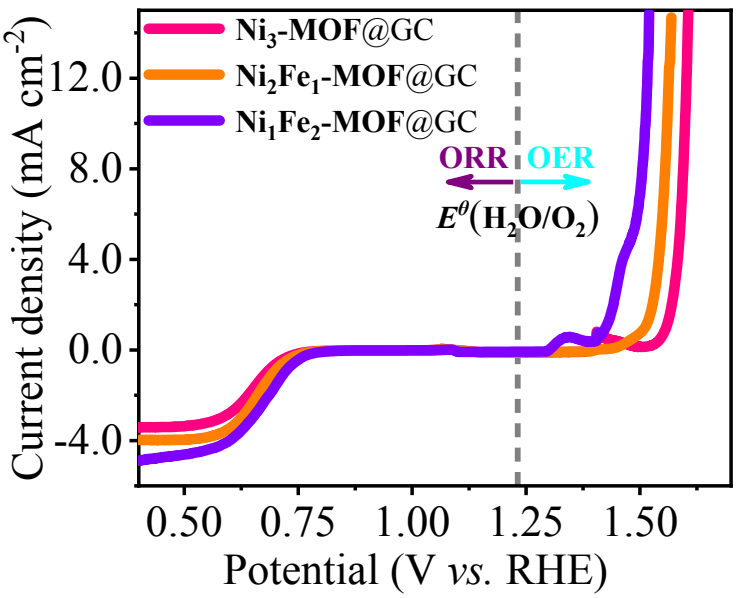

Figure S25. LSV OER/ORR curves of **Ni_3 -MOF**@GC, **Ni_2Fe_1 -MOF**@GC and **Ni_1Fe_2 -MOF**@GC in 0.1m KOH solution (pH 13).

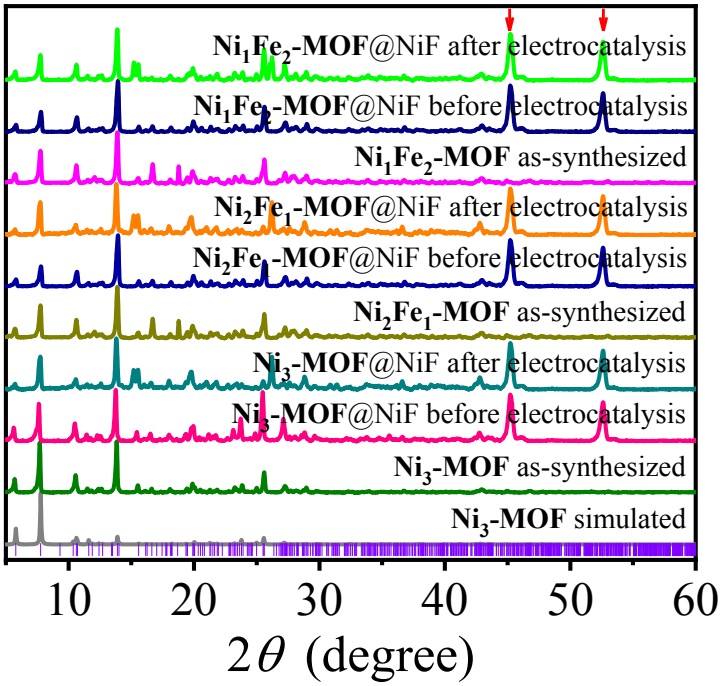

Figure S26. PXRD patterns of **Ni_3-MOF**@NiF, **Ni_2Fe_1-MOF**@NiF and **Ni_1Fe_2-MOF**@NiF before and after electrocatalysis testing (arrows indicate the characteristic diffraction peaks of Ni).

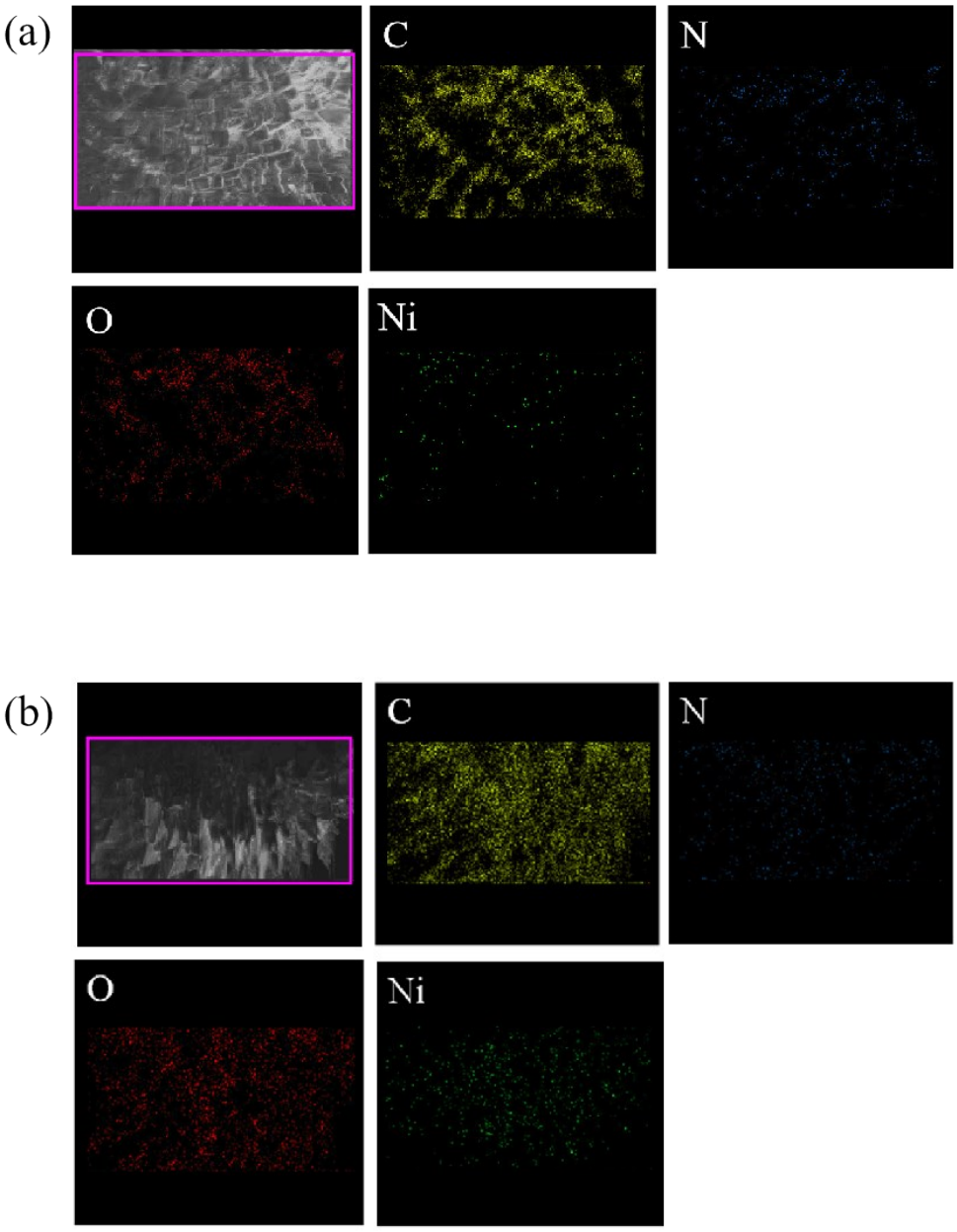

Figure S27. SEM-EDS mapping images of **Ni_3-MOF**@NiF (a) before (b) after electrocatalysis testing.

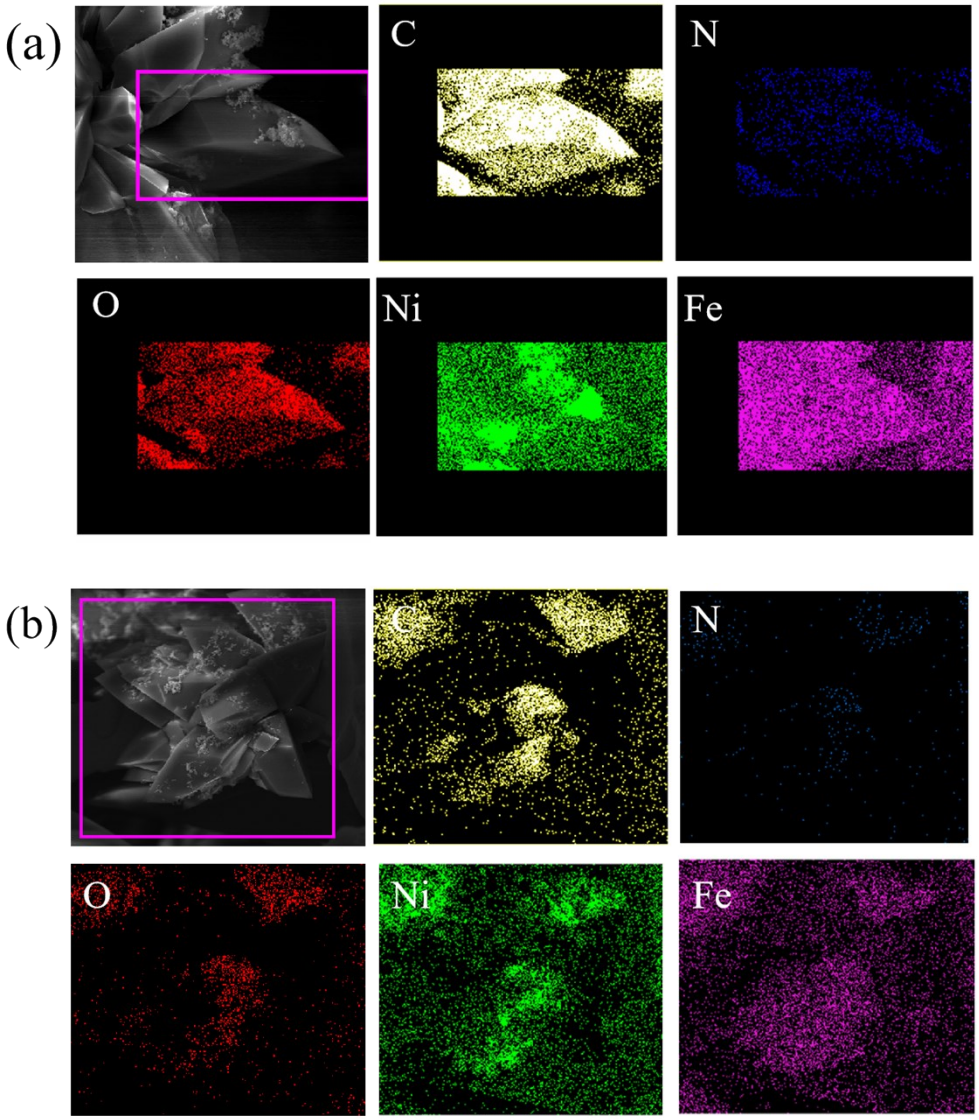

Figure S28. SEM-EDS mapping images of **Ni_2Fe_1-MOF**@NiF (a) before (b) after electrocatalysis testing.

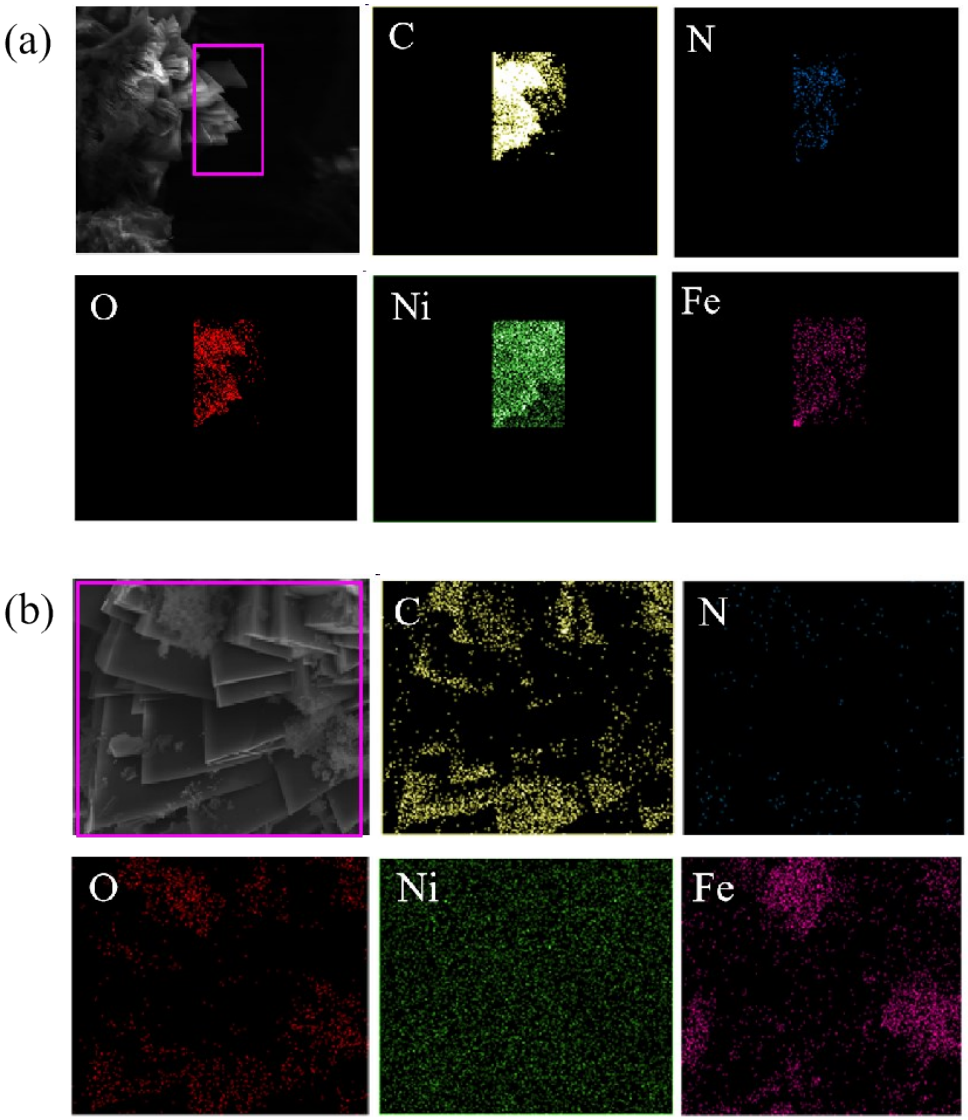

Figure S29. SEM-EDS mapping images of **Ni_1Fe_2-MOF**@NiF (a) before (b) after electrocatalysis testing.

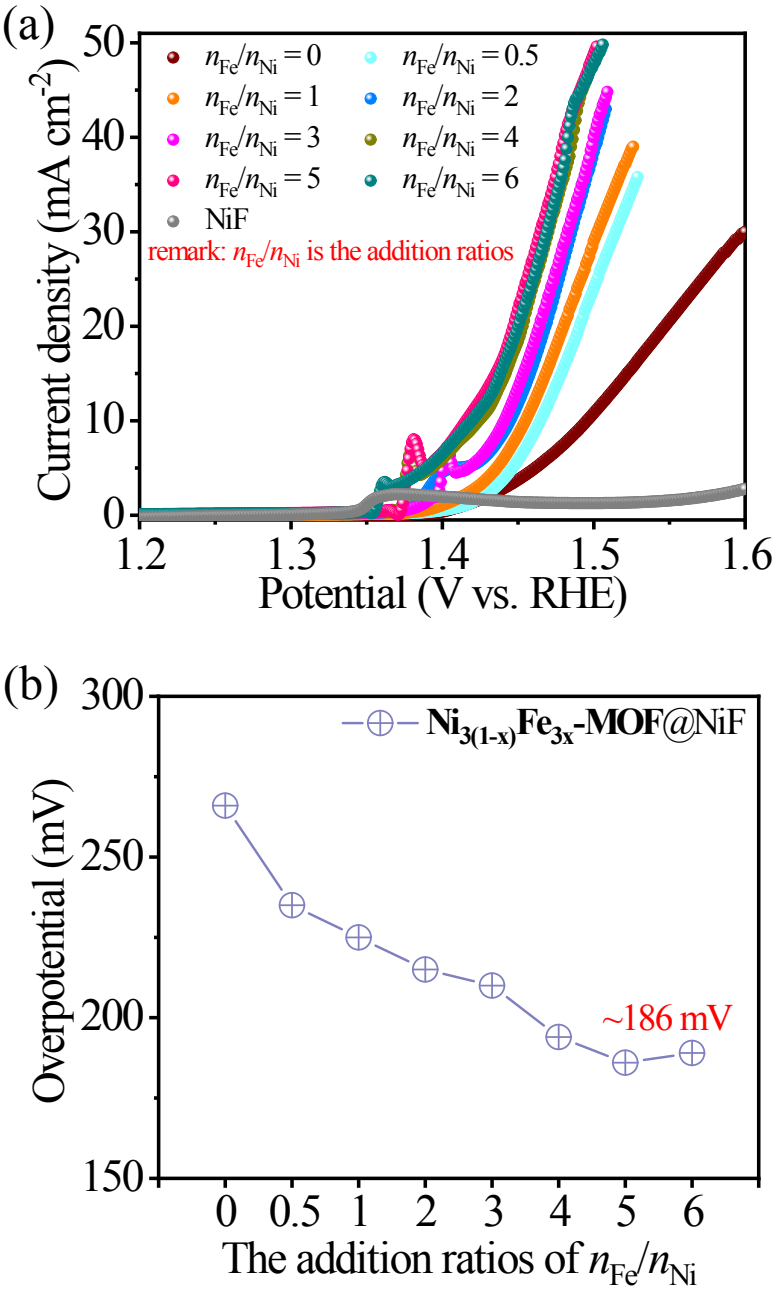

Figure S30. (a) LSV OER curves and (b) the corresponding $\eta_{OER\text{-}10}$ of **$Ni_{3(1-x)}Fe_{3x}$-MOF**@NiF in 0.1m KOH solution (pH 13).

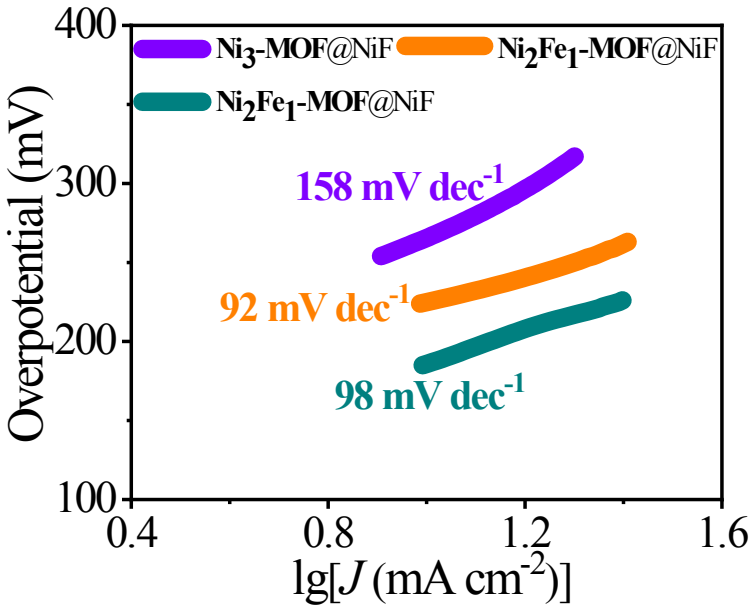

Figure S31. The OER Tafel plots of **Ni_3-MOF**@NiF, **Ni_2Fe_1-MOF**@NiF and **Ni_1Fe_2-MOF**@NiF.

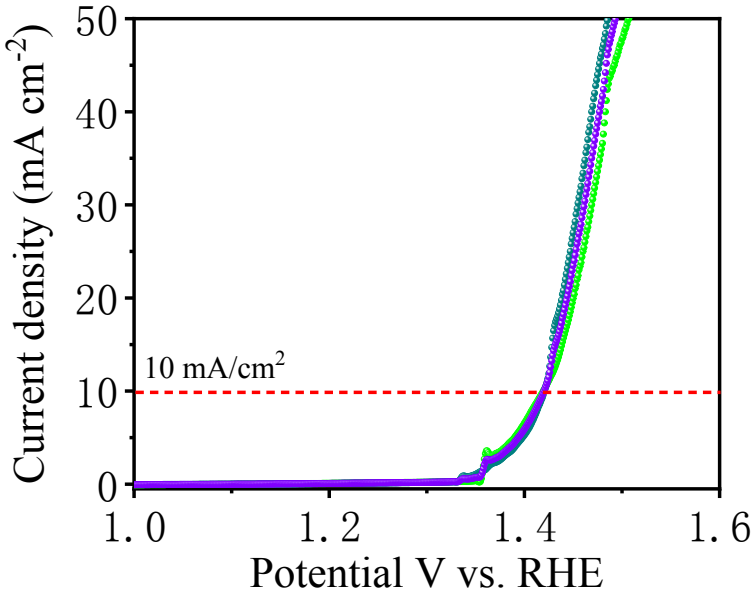

Figure S32. LSV OER curve of **Ni_1Fe_2-MOF**@NiF repeated three times in 0.1M KOH solution (pH 13).

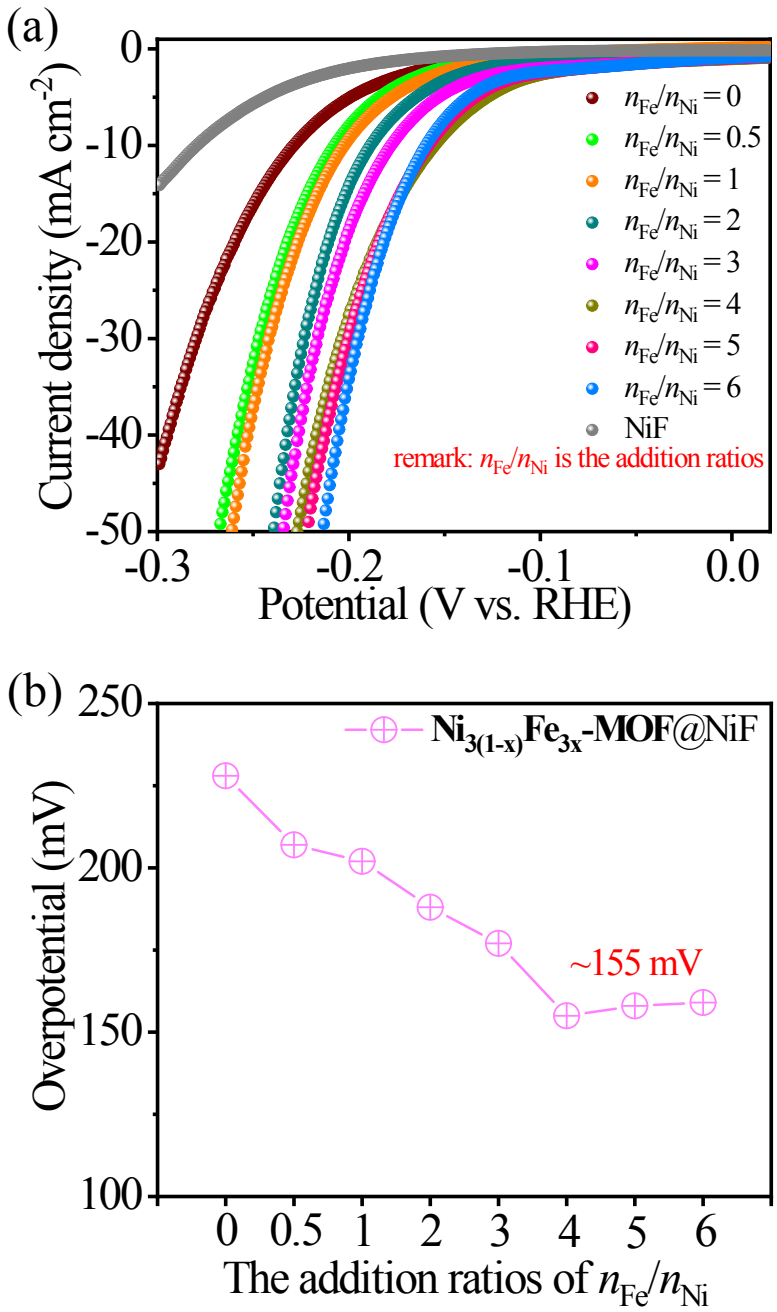

Figure S33. (a) LSV HER curves and (b) the corresponding $\eta_{\text{HER-10}}$ of **$Ni_{3(1-x)}Fe_{3x}$-MOF**@NiF in 0.1m KOH solution (pH 13).

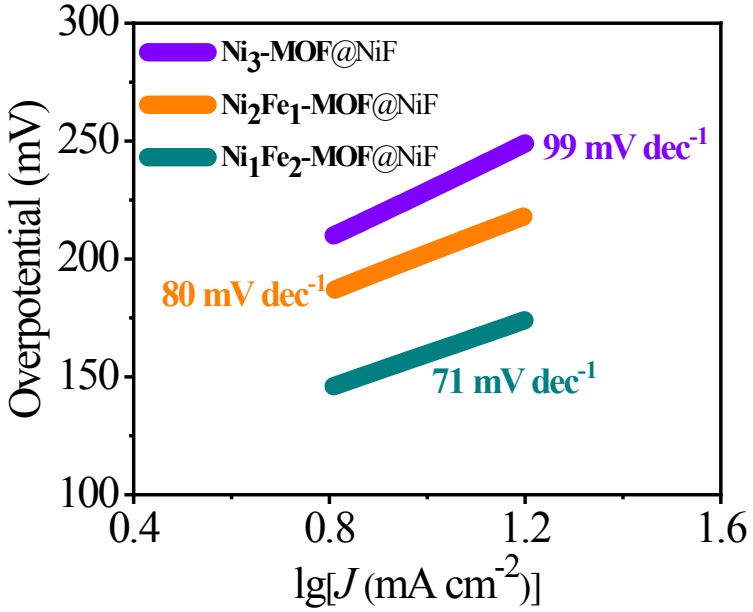

Figure S34. The HER Tafel plots of **Ni_3-MOF**@NiF, **Ni_2Fe_1-MOF**@NiF and **Ni_1Fe_2-MOF**@NiF.

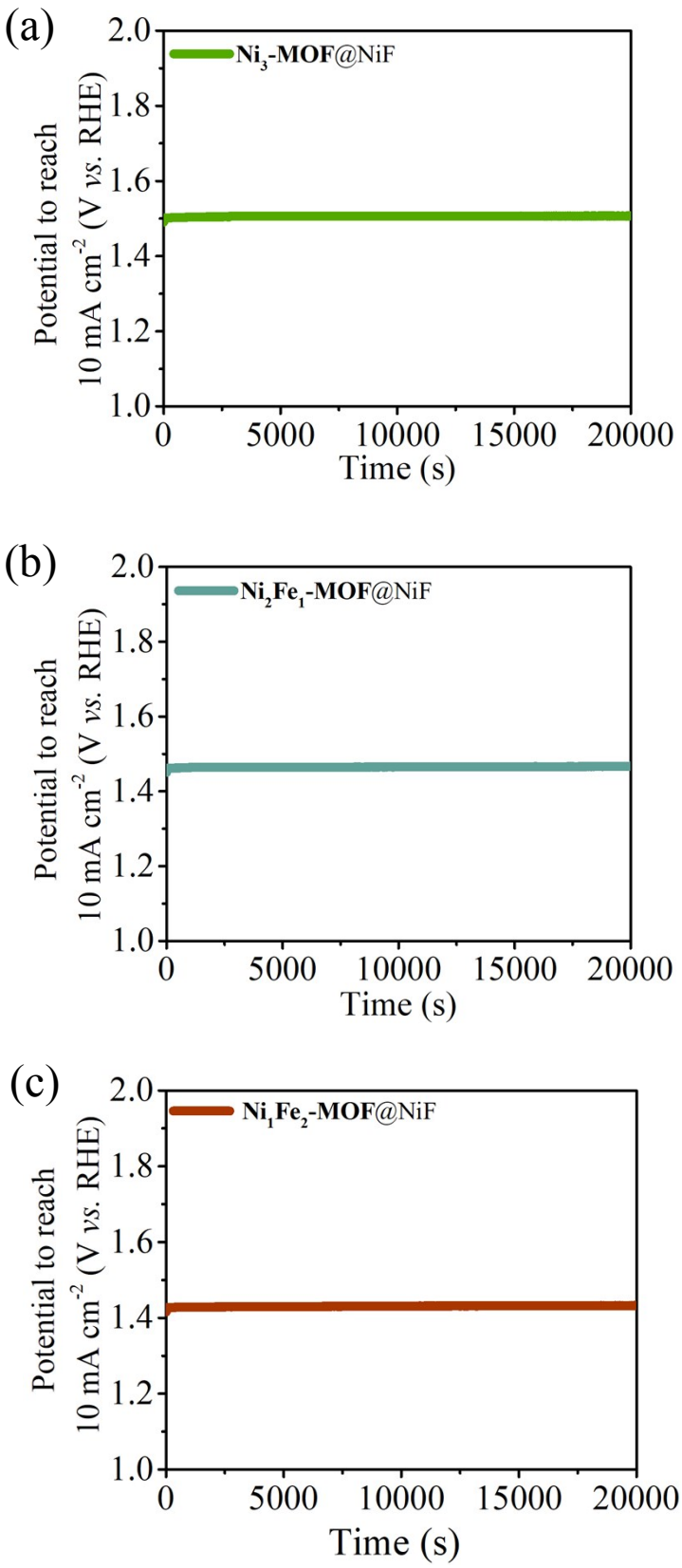

Figure S35. The OER chronopotentiometry curves of (a) **Ni_3-MOF**@NiF, (b) **Ni_2Fe_1-MOF**@NiF, and (c) **Ni_1Fe_2-MOF**@ NiF in 0.1M KOH solution (pH 13).

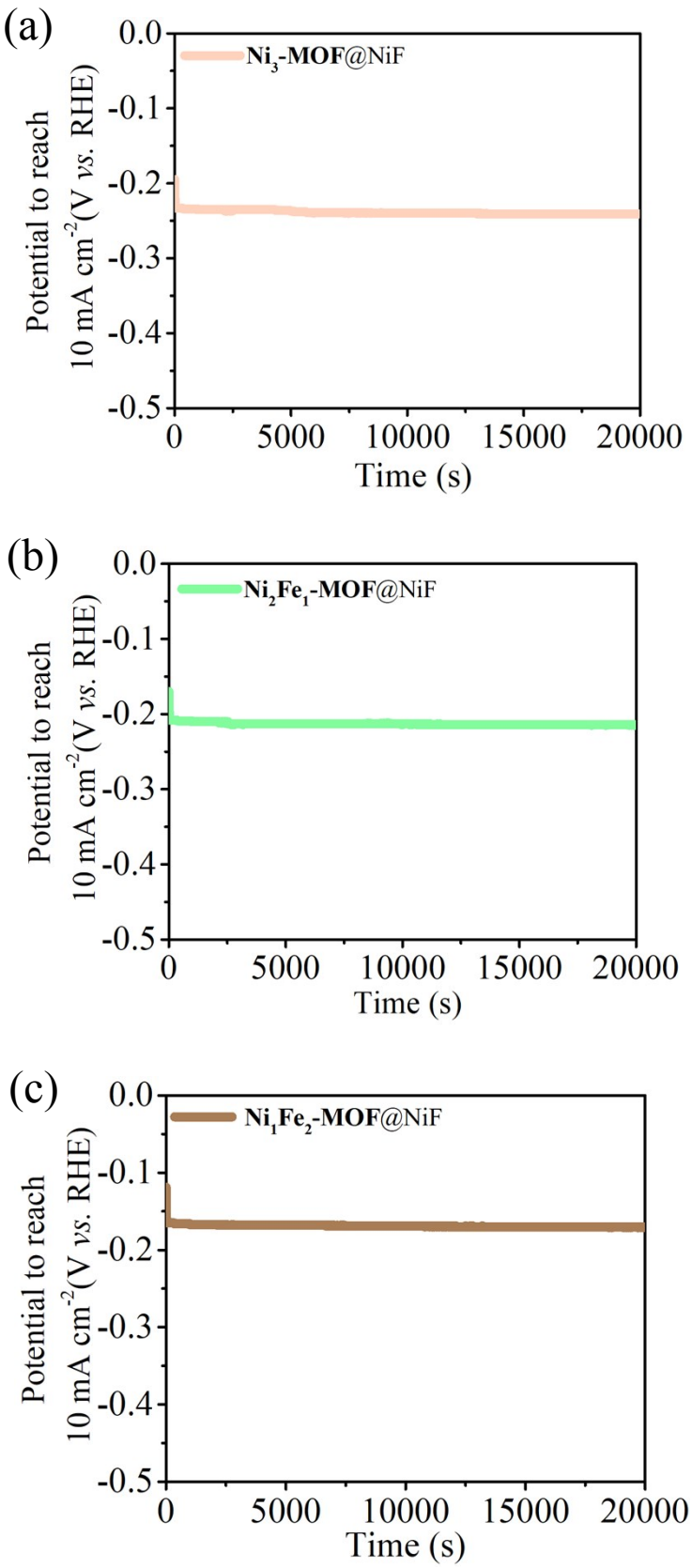

Figure S36. The HER chronopotentiometry curves of (a) **Ni_3-MOF**@NiF, (b) **Ni_2Fe_1-MOF**@NiF, and (c) **Ni_1Fe_2-MOF**@ NiF in 0.1M KOH solution (pH 13).

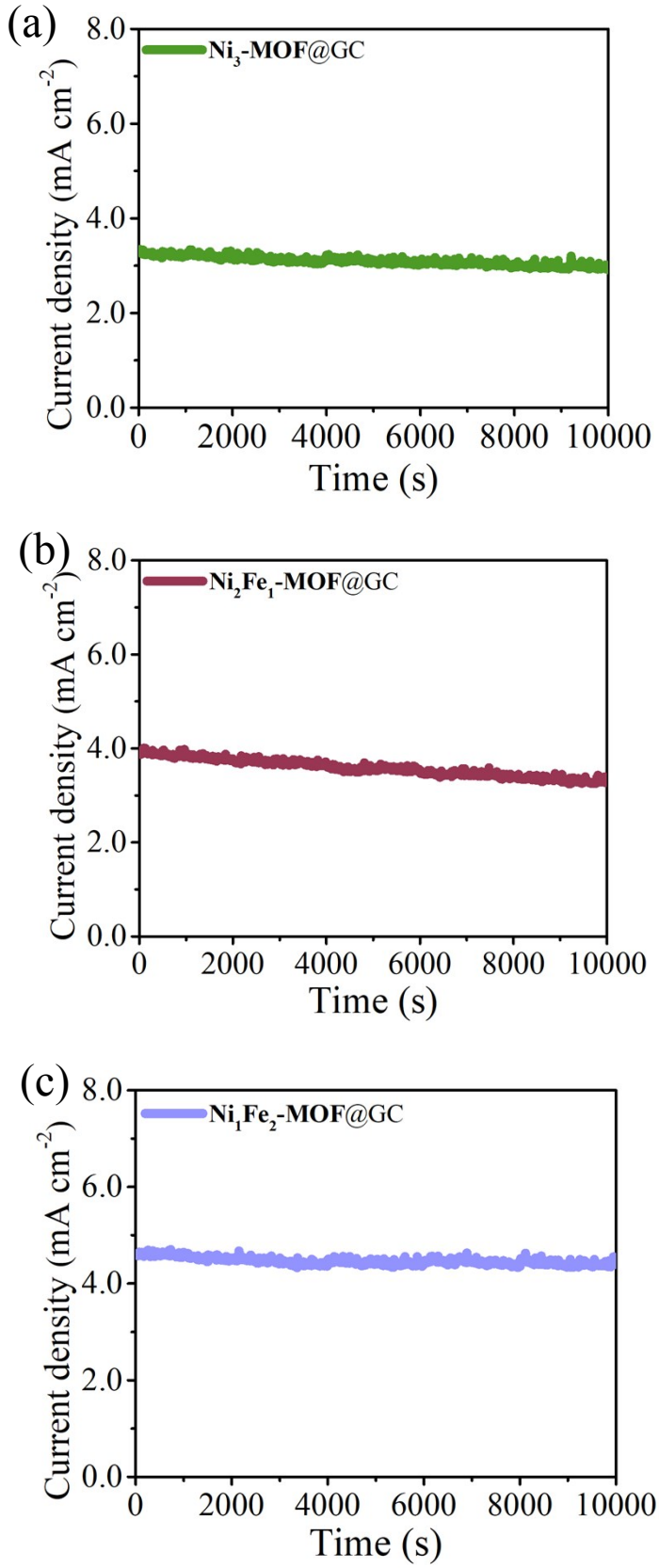

Figure S37. The ORR Chronoamperometry curves at the voltage of the electric current density of (a) **Ni_3-MOF**@GC, (b) **Ni_2Fe_1-MOF**@GC, and (c) **Ni_1Fe_2-MOF**@ GC in 0.1M KOH solution (pH 13).

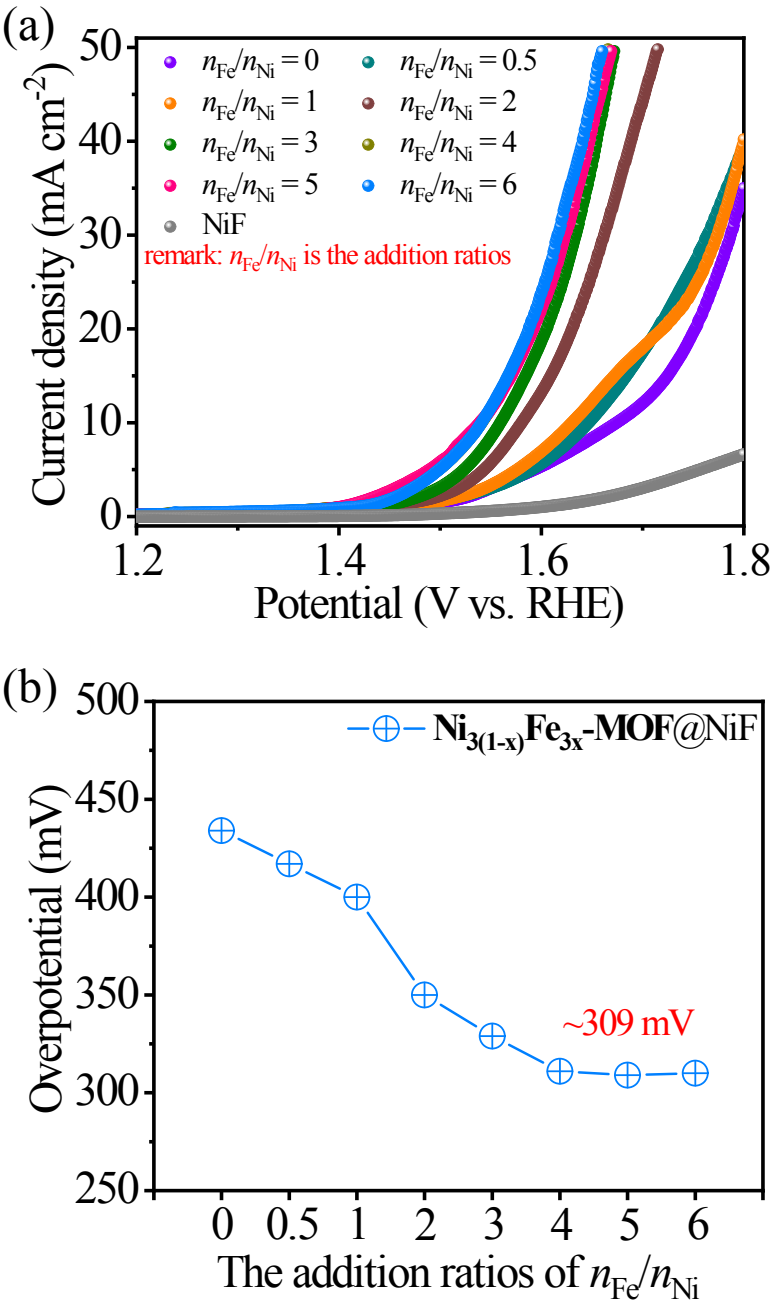

Figure S38. (a) LSV overall water splitting curves and (b) the corresponding $\eta_{\text{overall-10}}$ of **$Ni_{3(1-x)}Fe_{3x}$-MOF**@NiF in 0.1M KOH solution (pH 13).

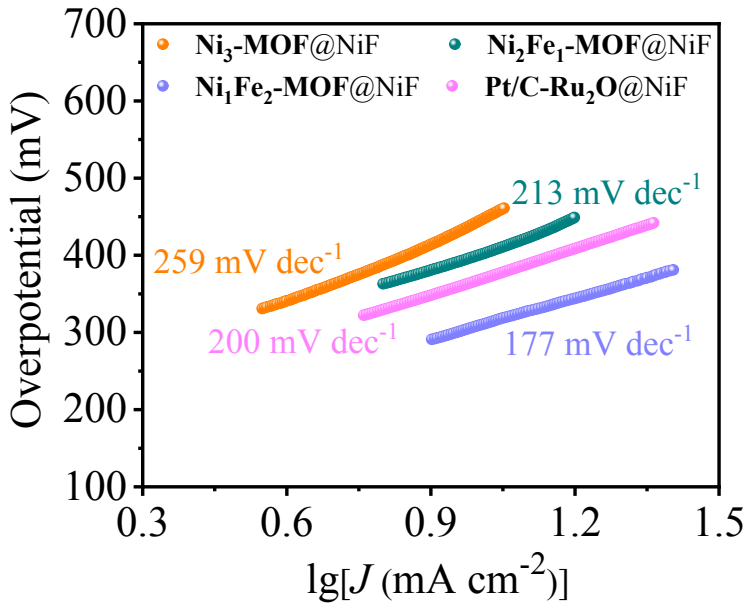

Figure S39. The overall water splitting Tafel plots of **Ni_3-MOF**@NiF, **Ni_2Fe_1-MOF**@NiF and **Ni_1Fe_2-MOF**@NiF.

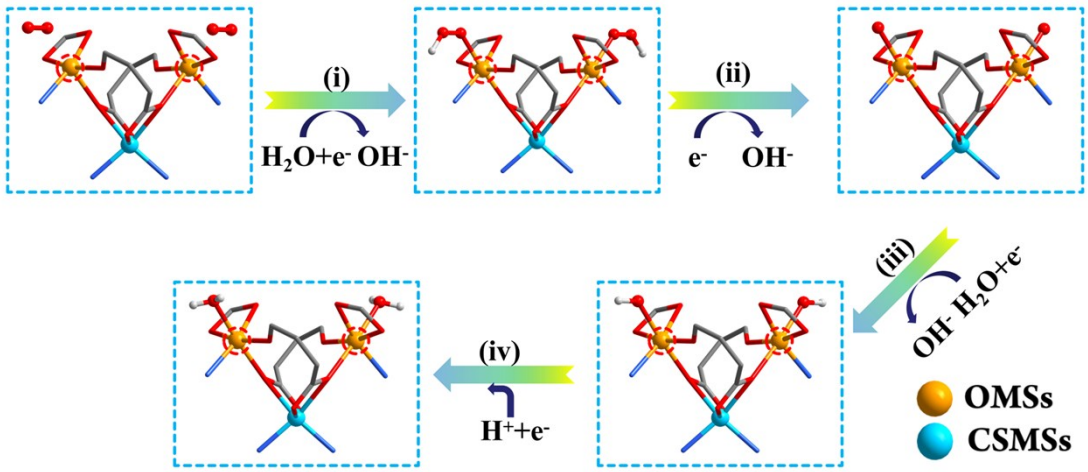

Figure S40. Four elementary OER steps on **$Ni_{3(1-x)}Fe_{3x}$-MOF** (x = 0, 0.33, 0.67 and 1) determined by DFT calculations.

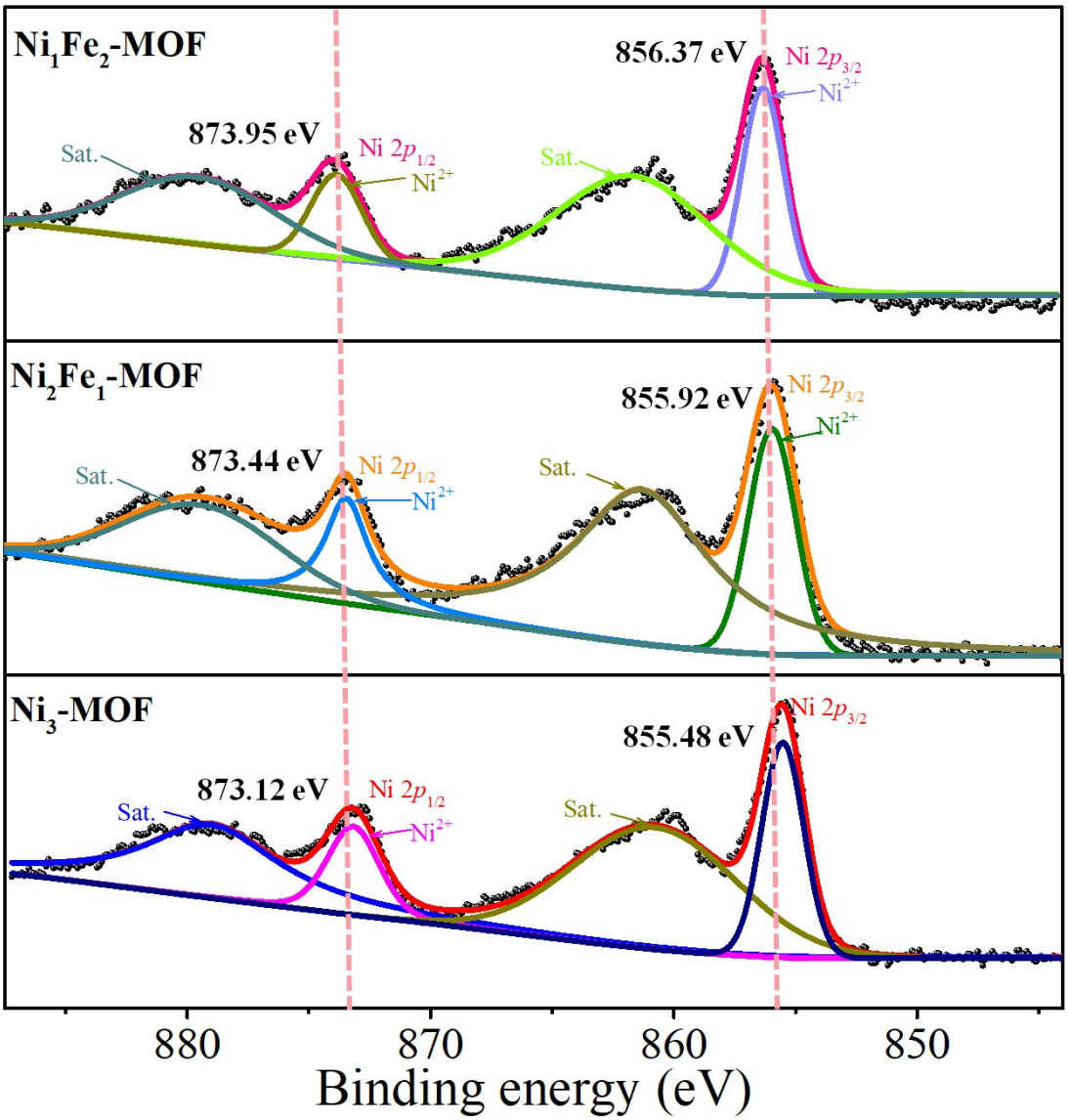

Figure S41. High-resolution XPS spectra of **Ni_3-MOF**, **Ni_2Fe_1-MOF** and **Ni_1Fe_2-MOF** for Ni 2*p* orbital.

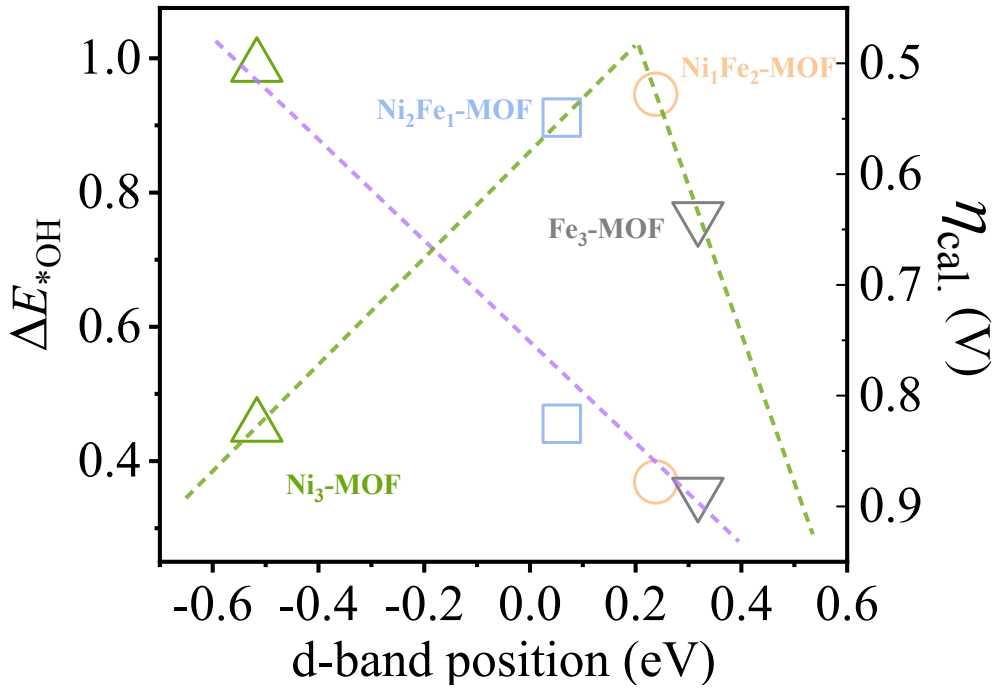

Figure S42. The calculated overpotentials of ORR with the d-band positions (the scaling relationship between the binding energy of *OH and the d-band positions was also plotted).

Table S1. Crystallographic Data and Structural Refinements for **Ni3-MOF**.

Compound	**Ni3-MOF**
Chemical formula	$C_{42}H_{30}O_{14}N_{12}Ni_3$
Formula weight	1102.91
Temperature (K)	100(10)
Crystal system	Monoclinic
Space group	*C*2/*c*
a/Å	9.87079 (13)
b/Å	30.4338 (4)
c/Å	16.92775 (17)
β/°	91.2934 (11)
V/Å^3	5083.89 (10)
Z	4
D_c /g cm^{-3}	1.441
R_{int}	0.0325
R_1 (>2σ)	0.040
wR_2 (all data)	0.1056
Completeness	0.996
GOF	1.055

Table S2. Selected bond lengths (Å) and angles (°) for Complexes.

Ni1—O1	2.0235 (15)	Ni2—O2D	2.1227 (15)
Ni1—O1A	2.0235 (15)	Ni2—O3E	1.9982 (16)
Ni1—O2	2.2364 (15)	Ni2—O5	2.0803 (15)
Ni1—O2A	2.2364 (15)	Ni2—O6	2.1353 (16)
Ni1—N6B	2.0304 (19)	Ni2—O7	2.0671 (16)
Ni1—N6C	2.0304 (19)	Ni2—N1	2.0670 (19)

O1—Ni1—O1^{i}	159.45 (9)	O2^{iv}—Ni2—O6	93.56 (6)
O1^{i}—Ni1—O2^{i}	61.50 (6)	O3^{v}—Ni2—O2^{iv}	85.77 (6)
O1—Ni1—O2	61.50 (6)	O3^{v}—Ni2—O5	167.00 (7)
O1—Ni1—O2^{i}	102.81 (6)	O3^{v}—Ni2—O6	104.28 (6)
O1^{i}—Ni1—O2	102.81 (6)	O3^{v}—Ni2—O7	91.14 (6)
O1—Ni1—N6^{ii}	95.72 (7)	O3^{v}—Ni2—N1	94.04 (7)
O1—Ni1—N6^{iii}	97.87 (7)	O5—Ni2—O2^{iv}	94.45 (6)
O1^{i}—Ni1—N6^{ii}	97.88 (7)	O5—Ni2—O6	62.72 (6)
O1^{i}—Ni1—N6^{iii}	95.72 (7)	O7—Ni2—O2^{iv}	175.86 (6)
O2^{i}—Ni1—O2	88.53 (8)	O7—Ni2—O5	87.95 (6)
N6^{ii}—Ni1—O2	156.61 (7)	O7—Ni2—O6	84.52 (6)
N6^{iii}—Ni1—O2^{i}	156.61 (7)	O7—Ni2—N1	94.98 (7)
N6^{iii}—Ni1—O2	91.85 (7)	N1—Ni2—O2^{iv}	87.99 (7)
N6^{ii}—Ni1—O2^{i}	91.85 (7)	N1—Ni2—O5	98.95 (7)
N6^{ii}—Ni1—N6^{iii}	96.89 (11)	N1—Ni2—O6	161.67 (7)

Table S3. Determining the metal content of $\mathbf{Ni_{3(1-x)}Fe_{3x}}$**-MOF** by ICP-MS.

n_{Fe}:n_{Ni} (addition)	0.5:1	1:1	2:1	3:1	4:1	5:1	6:1
Fe^{57} (ug/L)	34.10	50.84	73.28	75.53	96.76	105.83	110.48
Ni^{58} (ug/L)	130.88	104.17	80.42	77.67	67.43	53.58	56.75
n_{Fe}:n_{Ni} (ICP-MS)	0.26:1.00	0.49:1.00	0.75:1.00	0.99:1.00	1.46:1.00	2.01:1.00	1.98:1.00
$x = n_{Fe}/(n_{Fe} + n_{Ni})$ (ICP-MS)	0.21	0.33	0.43	0.5	0.6	0.67	0.67
$\mathbf{Ni_{3(1-x)}Fe_{3x}}$**-MOF**	$\mathbf{Ni_{2.4}Fe_{0.6}}$**-MOF**	$\mathbf{Ni_2Fe_1}$**-MOF**	$\mathbf{Ni_{1.8}Fe_{1.2}}$**-MOF**	$\mathbf{Ni_{1.5}Fe_{1.5}}$**-MOF**	$\mathbf{Ni_{1.2}Fe_{1.8}}$**-MOF**	$\mathbf{Ni_1Fe_2}$**-MOF**	$\mathbf{Ni_1Fe_2}$**-MOF**

Table S4. Comparison of the OER activities of MOFs in 0.1 M KOH solution.

Catalysts	Overpotential (mV) (at J=10 mA cm^{-2})	Tafel slope (mV dec^{-1})	Substrate	Binder	Reference
Ni_3-MOF	369	47	GC	Nafion	This work
	266	158	Ni foam	Null	
Ni_2Fe_1-MOF	330	46	GC	Nafion	
	225	92	Ni foam	Null	
Ni_1Fe_2-MOF	283	41	GC	Nafion	
	186	98	Ni foam	Null	
4.3%-NiFe-MOF	210 (at J=200 mA cm^{-2})	68	Ni foam	Null	*Nat. Energy* **2019,** *4,* 115.
NCF MOF	190	49	Ni foam	Nul	*Adv. Funct. Mater.* **2018,** *28*, 1802129.
	320	NA	GC	Nafion	
Fe:2D-Co-NS	211	43	Ni foam	Null	*Angew. Chem. Int. Ed.* **2018,** *57*, 4632.
	282	59	GC	Nafion	
Fe_3-Co_2	283	43	GC	Nafion	*J.Am. Chem. Soc.***2017,** *139*, 1778.
	225	48	Ni foam	Nafion	
	237	79	Cu foam	Nafion	
NiFe-MOF	240	34	Ni foam	Null	*Nat. Commun.* **2017,** *8*, 15341.
CTGU-10c2	240	58	GC	Nafion	*Angew. Chem. Int. Ed.* **2019,** *58*, 4227.
Pt3.2%@NiNSMOFs	298	107	RRDE	Nafion	*Appl. Catal. B-Environ.* **2019,** *245*, 389.
NNU-23	365	81.2	CC	Nafion	*Angew. Chem. Int. Ed.* **2018,** *57*, 9660.
Fe_2Co-MOF	402	81.2	GC	Nafion	*Inorg. Chem.* **2020,** 59, 6078.
$Ti_3C_2T_x$–CoBDC	410	48.2	GC	Nafion	*ACS Nano,* **2017,** *11*, 5800.
MAF-X27-OH	461	66	GC	Nafion	*J. Am. Chem. Soc.* **2016,** *138,* 8336
Co-WOC-1	390 (at J=1 mA cm^{-2})	128	GC	Nafion	*Angew. Chem. Int. Ed.* **2016,** *55*, 2425.
Co-ZIF-9	510 (at J=1 mA cm^{-2})	93	FTO glass	Nafion	*Nanoscale* **2014**, *6,* 9930-9934.
IrO_2/C(52 wt%)	310	97	Cu foil	Null	*J. Am. Chem. Soc.* **2014,** *136,* 13925.
RuO_2	320	62	GC	Nafion	*Angew. Chem. Int. Ed.* **2019,** *58*, 4227.

Table S5. Comparison of the HER activities of MOFs in 0.1 M KOH solution.

Catalysts	Overpotential (mV) (at J=10 mA cm^{-2})	Tafel slope (mV dec^{-1})	Substrate	Binder	Reference
Ni_3-MOF	537	133	GC	Nafion	This work
	229	99	Ni foam	Null	
Ni_2Fe_1-MOF	484	131	GC	Nafion	
	203	80	Ni foam	Null	
Ni_1Fe_2-MOF	373	107	GC	Nafion	
	155	71	Ni foam	Null	
NCF MOF	110	114	Ni foam	Null	*Adv. Funct. Mater.* **2018,** 28, 1802129.
	270	NA	GC	Nafion	
HUST-200	131	51	GC	Nafion	*ACS Appl. Mater. Interfaces* **2018,** 10, 31498.
NiFe-MOF	134	NA	Ni foam	Null	*Nat. Commun.* **2017,** 8, 15341.
Fe_2Zn-MOF	221	174	GC	Nafion	*Inorg. Chem.* **2020,** 59, 6078.
IrO_2/C(20 wt%)	122	252.6	GC	Nafion	*Inorg. Chem.* **2020,** 59, 6078.

Table S6 Comparison of the ORR activities of MOFs in in 0.1 M KOH solution.

Catalysts	E_{onset} (V *vs* RHE)	$E_{1/2}$ (V *vs* RHE)	J_{lim} (mA cm^{-2})	Electron transfers Number (*n*)	Reference
Ni_3-MOF	0.792	0.651	-3.42	2.49	This work
Ni_2Fe_1-MOF	0.795	0.663	-3.99	3.82	
Ni_1Fe_2-MOF	0.802	0.676	-5.02	3.96	
$(G\text{-}dye\text{-}FeP)_n$ MOF	0.93	0.78	-6.3	3.82	*J.Am. Chem. Soc.* **2012,** 134, 6707.
4.3%-NiFe-MOF	0.92	0.83	-5.2	3.8	*Nat. Energy* **2019,** 4, 115.
PcCu-O_8-Co/CNT	0.86	0.83	-5.3	3.93	*Angew.Chem. Int.Ed.* **2019,** 58 ,10677.
MCCF/NiMn-MOFs	0.85	0.73	-5.6	3.86	*Angew. Chem. Int. Ed.* **2020,** 59, 18234.
PCN-226(Co)	0.83	0.75	-2.9	3.3	*J.Am. Chem. Soc.* **2020,**142, 15386.
[$Ni_3(tha)_2$]	0.82	0.67	-2.5	2.25	*Nat. Commun.* **2016,** 7, 10942.
Ni/Co-MOF	0.76	0.62	-4.5	3.7	*Nano Lett.* **2017,** 9, 43.
Co-Al-PMOF	0.75	0.55	-0.6	2.9	*Chem. Commun* **2017,** 53, 6496.
HKUST-1	0.71	0.56	-4.9	1.74	*Angew. Chem. Int. Ed.* **2016,** 55, 15301.
$(Fe\text{-}P)_n$ MOF	0.7	0.57	-2.6	1.93	*J.Am. Chem. Soc.* **2012,** 134, 6707.
MIL-100(Fe)	0.7	0.59	-3.8	2.1	*Chin. J. Catal.* **2014,** 35, 185.

Table S7. The value of electron transfer numbers of **Ni_3-MOF**@GC, **Ni_2Fe_1-MOF**@GC, and **Ni_1Fe_2-MOF**@GC in O_2-saturated 0.1 M KOH solution.

Sample	**Ni_3-MOF**	**Ni_2Fe_1-MOF**	**Ni_1Fe_2-MOF**
Electron Transfer Numbers	2.49	3.82	3.96

Table S8. Comparison of the ΔE ($\Delta E = E_{OER} - E_{1/2}$) activities of MOFs and recently reported active catalysts.

Catalyst	E_{ORR} (V) (Half-wave Potential)	E_{OER} (V) (at J=10 mA cm^{-2})	$\Delta E = E_{ORR} - E_{OER}$ (V)	Reference
Ni_3-MOF	0.651	1.599	0.948	This work
Ni_2Fe_1-MOF	0.663	1.56	0.897	
Ni_1Fe_2-MOF	0.676	1.513	0.837	
4.3%-NiFe-MOF	0.83	1.53 (at J=2000mA cm^{-2})	0.7	*Nat. Energy,* **2019,** 4, 115.
MCCF/NiMn-MOFs	0.73	1.51	0.78	*Angew. Chem. Int. Ed.* **2020,** 59, 18234.

Table S9. Comparison of the water splitting activities of MOFs.

Catalysts	Water splitting potential (V) @10mA cm^{-2}	Overpotential (mV) OER @10mA cm^{-2}	Overpotential (mV) HER @10mA cm^{-2}	Substrate	Binder	Reference
Ni_3-MOF	1.675	266	229	Ni foam	Null	*This work*
Ni_2Fe_1-MOF	1.631	225	203			
Ni_1Fe_2-MOF	1.54	186	155			
Pt/C-RuO_2	1.597	427	111	Ni foam	Null	
Ni/Fe-MOF	1.55	240	134	Ni foam	Null	*Nat. Commun.* **2017,** 8, 15341.
NiFe-MS/MOF	1.61 (at *J*=50 mA cm^{-2})	230 (at *J*=50mA cm^{-2})	156 (at *J*=50mA cm^{-2})	Ni foam	Null	*Adv.Sci.* **2020,** 7, 2001965.
MFN-MOFs (2:1)	1.495	235 (at *J*=50mA cm^{-2})	79	Ni foam	Null	*Nano Energy* **2019,** 57, 1.
D-Ni-MOF	1.5	219	101	Ni foam	Null	*Small* **2020,**16, 1906564.
NFN-MOF	1.56	240	87	Ni foam	Null	*Adv. Energy Mater.* **2018,** 1801065.
FeNi(BDC)(DMF,F)	1.58	227 (at *J*=60mA cm^{-2})	234 (at *J*=60mA cm^{-2})	Ni foam	Null	*Applied Catalysis B: Environmental* . **2019,** 258, 118023.

Table S10. Comparison of the trifunctional activities of MOFs and recently reported active catalysts in 0.1M KOH solution.

Catalysts	Overpotential (mV) OER@10mA cm^{-2}	Overpotential (mV) HER@10mA cm^{-2}	$E_{1/2}$ (V *vs* RHE) ORR	Reference
Ni_3-MOF	369	537	0.651	*This work*
Ni_2Fe_1-MOF	330	484	0.663	
Ni_3Fe_2-MOF	283	373	0.676	
P-3G	320	230	0.82	*J. Mater. Chem. A.* **2019**, *7*, 2048.
FeCo/Co_2P@NPCF	330	260	0.79	*Adv. Energy. Mater.* **2020**, *10*, 1903854.
Fe_3C-Co/NC	340	238	0.885	*Adv. Energy Mater.* **2019**, 29, 1901949.
GH-BGQD2	370	130	0.87	*Adv. Energy Mater.* **2019**, *9*, 1900945.
PPy/FeTCPP/Co	380	240	0.86	*Adv. Funct. Mater.* **2017**, *27*, 1606497.
G@N-MoS_2	390	243	0.716	*Adv. Mater.* **2018**, *30*, 1705110.
Co-CoO/N-rGO	390	330	0.78	*Adv. Funct. Mater.* **2015**, *25*, 5799.
Co/CoO@Co-N-C-800	392	413	0.787	*Chem. Commun.* **2016**, *52*, 5946.
A-PBCCF-H	410	224	0.76	*Nano Energy* **2017**, *32*, 247.
SHG	410	310	0.87	*Adv. Mater.* **2017**, *29*, 1604942.
CoO@Co/N-rGO	420	237	0.81	*J. Mater. Chem. A* **2017**, *5*, 5865.
Fe-N_4 SAs/NPC	430	202	0.885	*Angew. Chem. Int. Ed.* **2018**, *57*, 8614.
Co-Co_9S_8@SNCNTs-900	450	240	0.81	*Nano Energy* **2019**, *56*, 724–732.
C_{60}-$SWCNT_{15}$	460	380	0.84	*J. Am. Chem. Soc.* **2019**, *141*, 11658.
GO-PANi-FP	560	520	0.72	*Angew. Chem. Int. Ed.* **2016**, *55*, 13296.
GO-PANi31-FP	590	520	0.72	*Angew. Chem.* **2016**, *128*, 13490.